DESIGN CONCEPTS for a HIGH-IMPEDANCE NARROW-BAND 42 GHz POWER TWT using a "FUNDAMENTAL /FORWARD" LADDER-BASED CIRCUIT

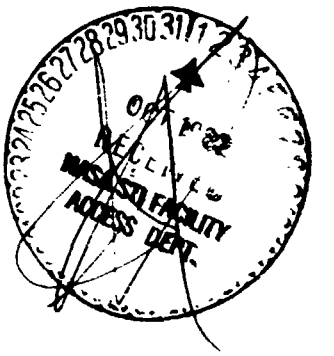

FINAL REPORT

August 1980

A. Karp

Prepared for:

NATIONAL AERONAUTICS and SPACE ADMINISTRATION

NASA Lewis Research Center

Contract NAS 3-21930

("Study of Karp Slow-Wave Structure")

April 1979 - March 1980

Contractor J.O. No. 19128

Varian Associates, Inc.
Palo Alto Microwave Tube Division
611 Hansen Way
Palo Alto, California 94303

DESIGN CONCEPTS FOR A HIGH-IMPEDANCE NARROW-BAND 42 GHz POWER TWT USING A "FUNDAMENTAL/FORWARD" LADDER-BASED CIRCUIT

Final Report

August 1980

A. Karp

Prepared for:
NATIONAL AERONAUTICS AND SPACE ADMINISTRATION
NASA Lewis Research Center
Contract NAS 3-21930

("Study of Karp Slow-Wave Structure")
April 1979 - March 1980

Contractor J.O. No. 19128

Varian Associates, Inc.
Palo Alto Microwave Tube Division
611 Hansen Way
Palo Alto, California 94303

TECHNICAL REPORT STANDARD TITLE PAGE

1. Report No.	2. Government Accession No.	3. Recipient's Catalog No.
CR 165282		

4. Title and Subtitle	5. Report Date
DESIGN CONCEPTS for a HIGH-IMPEDANCE NARROW-BAND 42 GHz POWER TWT using a "FUNDAMENTAL/FORWARD" LADDER-BASED CIRCUIT ("Study of Karp Slow-Wave Structure")	August 1980
	6. Performing Organization Code
7. Author(s)	8. Performing Organization Report No.
A. KARP	J.O. 19128
9. Performing Organization Name and Address	10. Work Unit No.
Varian Associates 611 Hansen Way Palo Alto, CA 94303	541-02-12 - YOT 8343
	11. Contract or Grant No
	NAS 3-21930
	13. Type of Report and Period Covered
12. Sponsoring Agency Name and Address	Contractor Report April 1979 – March 1980
National Aeronautics and Space Administration Lewis Research Center Cleveland, Ohio 44135	14. Sponsoring Agency Code

15 Supplementary Notes

Project Manager, Dr. James A. Dayton, Jr., NASA Lewis Research Center, Cleveland, Ohio
Office Code 6231 Document Release Authorization 2 March 1981

16. Abstract

A study program was completed in support of an eventual low-cost, narrow-band, millimeter-wave space-communications TWT of novel design. Cold-test interaction-structure scale models were investigated and analyses were undertaken to predict the electrical and thermal response of the hypothetical 200-W TWT at 42 GHz and 21 kV beam voltage.

Following a NASA suggestion, an intentionally narrow instantaneous bandwidth (1%, with the possibility of electronic tuning of the center frequency over several percent) was sought with a highly dispersive, high-impedance "forward-wave" interaction structure based on a ladder (for economy in fabrication) and non-space-harmonic interaction, for a high gain rate and a short, economically focused tube. The "TunneLadder" interaction structure devised combines ladder properties with accommodation for a pencil beam. Except for the impedance and bandwidth, there is much in common with the millimeter-wave helix-TWTs which provided the idea of diamond support rods. The benefits of these are enhanced in the TunneLadder case because of spatial separation of beam-interception and rf-current heating.

(Continued next page)

17 Key Words (Selected by Author(s))	18 Distribution Statement
Millimeter-wave amplifier Narrow-band communications TWT Slow-wave circuit Ladder-based interaction structure Diamond support rods	Unclassified – Unlimited

19 Security Classif (of this report)	20 Security Classif (of this page)	21 No. of Pages	22. Price*
Unclassified	Unclassified	v + 71	

*For sale by the Clearinghouse for Federal Scientific and Technical Information, Springfield, Virginia 22151

15. Abstract (Continued)

In advance of possible future development of a TunneLadder TWT, consideration was given (in varying degrees) to the following concerns: interaction impedance, sensitivities to dimensional deviations, extraneous modes of propagation, prior art, circuit attenuation, temperature rises, rf breakdown, small- and large-signal gain, efficiency, fabrication techniques, input/output couplers, and "severs".

TABLE OF CONTENTS

LIST OF ILLUSTRATIONS

LIST OF ILLUSTRATIONS (CONT'D)

FOREWORD

Acknowledgement is hereby made to NASA-LeRC personnel, Dr. Henry G. Kosmahl, for identifying the applications need, originating the underlying design approach and instigating its further development, and Dr. James A. Dayton, Jr., for facilitating the pursuit of contract objectives.

At Varian Associates, Inc., Palo Alto Microwave Tube Division, Division R and D operation, John W. Fenwick and Gary A. Biggs undertook the various modifications of the interaction-structure models of Figures 1, 6 and 12 and obtained all the cold-test data pertaining to them. The graphical presentation of these data is due to F. Ruth Walker who also contributed the equivalent-circuit analyses summarized in Section 4.5. The small- and large-signal analyses of Sections 6.1 through 6.4 were the contribution of Thomas J. Grant while George E. Wendell was responsible for the VULCAN-program thermal modeling reviewed in Section 7.5.

The recent advances in millimeter-wave helix-TWT design with helices bonded to diamond support rods, which have an essential bearing on the subject contract efforts, were directed and communicated by Andre E. Jacquez, Helix Amplifier Tube Operation.

1.0 SUMMARY

This contract final report reviews an eleven-month study program relating to an unconventional low-cost traveling-wave amplifier for narrow-band space communications at millimeter-wave frequencies such as 42 GHz. The work involved the design, construction and testing of scale models of periodic slow-wave interaction structures, data processing, and other analytical procedures supporting the possible future development of a working tube based on the principles proposed and evaluated.

The basic design premises were originated at NASA-LeRC, by Dr. H.G. Kosmahl, who proposed capitalizing on the narrow bandwidths (1% or thereabout) of the systems addressed to effect a TWA that was smaller and cheaper than a conventional coupled-cavity TWA might be for 42 GHz -- and at least 200 W of CW output power. This concept entailed the selection of a highly dispersive narrow-band interaction structure, of the "forward-wave" type intended for non-space-harmonic interaction. Because of all these features, a high gain per unit length should result, leading to a short tube, a relatively small yoke-type permanent magnet for focusing, and a lessened impact of circuit attenuation on gain and efficiency. The results of the subject study program support these claims and objectives.

The NASA-LeRC slow-wave circuit recommendation was a ladder-based structure, such as might be made inexpensively, and without cumulative errors in periodicity, by winding of tape, photo-etching of foil, etc. Experimental evaluation of S-band models of such circuits, with the (thin) ladder in flat form, was undertaken as a useful preliminary. The ladder was subsequently modified to accommodate a practical pencil beam (consistent with the high-power objective) and diamond rods (simulated by Stycast 5 in the models) were added for support and cooling. The resulting "TunneLadder" design thus owes much to recent concepts in millimeter-wave helix-TWT design. structurally and electrically -- excepting only the impedance, dispersion and bandwidth. Thermally, the TunneLadder design (with a quasielliptical beam tunnel) has the added advantage of spatial separation of beam-interception and rf-current heating.

In support of the proposed interaction-structure design, interaction impedance, sensitivities to dimensional deviations, extraneous modes of propagation, and prior art were critically investigated. Circuit attenuation and power-handling capability were projected analytically, as were small- and large-signal gain, bandwidth, "saturated" efficiency, and rf voltage stresses. For these purposes, a beam voltage, microperveance, and diameter of 21 kV, 0.06, and 0.4 mm, respectively, were assumed. As intended, predicted instantaneous bandwidths are narrow (1 to 2%, according to how defined) but electronic tuning of the center frequency (at the rate of $\pm$ 2% for $\pm$ 4 kV) should be practicable.

Starting with a data update on the rf loss and breakdown properties of Type II A diamond, further development efforts focused on ladder-fabrication techniques, input/output transitions between rectangular waveguide and the interaction structure, and a possible "sever", are needed to bridge the gap between the present body of cold-test/analytic results and an operating "TunneLadder" TWT.

2.0 INTRODUCTION

2.1 GENERAL

This Final Report covers an eleven-month study program supporting the eventual development of an unconventional, narrow-band communications TWT outputting at least 200 W, CW, at 42 GHz (or other nearby center frequency). The principal tasks of the study program were the construction and "cold-testing" of scaled-up interaction-circuit models and analytical projections of various aspects of their potential performance in a 42 GHz TWT.

These base-line efforts were motivated by interest in a lower-cost alternative to the coupled-cavity TWTs that are conventionally considered for these frequencies and power levels. As discerned by H. G. Kosmahl in 1977, more than 1% of instantaneous bandwidth (defined "1 dB down") is seldom required in a millimeter-wave communications amplifier, paving the way to favor low cost and/or high interaction impedance over bandwidth potential for the candidate interaction structure. The high interaction impedance, leading to high gain per unit length, and a physically short tube, should lessen the impact of circuit attenuation on efficiency and permit beam focusing by a yoke-type permanent magnet of modest size and weight.

To maximize the amplifier gain rate obtainable over the specified bandwidth, non-space-harmonic interaction was recommended, requiring the slow-wave circuit to be "forward-wave" (codirected phase and group velocities for the non-space-harmonic wave) as is the helix. This type of interaction also tends to require a fine circuit pitch, implying fragile structural elements, but the recommendation of the moderately high beam voltage of 21 kV (v/c = 0.28) would provide some relief here without exacerbating the insulation problems of the amplifier package. On the basis of theoretical projections for a simplified circuit model, Kosmahl predicted that a tape-ladder circuit dimensioned to operate at about six periods per guide wavelength, and ridge loaded to achieve at this point a group velocity in the vicinity of 0.05 c, would meet the impedance/hot-bandwidth requirements. This has since been substantiated.

The scope of the study program included the construction of a "reference" circuit for cold-test evaluations at S-band frequencies. Though it was highly simplified and designed without regard to thermo-mechanical or electron-optical concerns, the measurements made while changing circuit parameters promoted fundamental understanding and helped prognose ultimate limitations. The results here subsequently provided guidance for the design and construction of a "practical" circuit model (scaled 16:1) developed around a pencil beam with due concern for eventual fabrication techniques, mechanical stability, and the removal of heat due to both electron interception and rf dissipation.

Also within the scope of the study program were small- and large-signal gain/bandwidth/efficiency projections based on suitable electron-beam parameters, data obtained from the "cold tests", and considered estimates of eventual circuit attenuation. Studies were also made regarding sensitivity to dimensional deviations, rf voltage stresses, and the temperature rises likely to occur under operating conditions. The possible effects of the extraneous modes of propagation of the "practical" structure received amr consideration. Approaches to the eventually required input/output waveguide/periodic-structure couplers, and "sever", received some attention but no "hardware" construction was initiated.

The total of the contract effort may be viewed as having birthed a promising new design for a reproducible, efficient, narrow-band power amplifier at 42 GHz, and laid analytical and experimental foundations for optimizing its design for eventual manufacture and service in millimeter-wave communications links

2.2 ORIGINS

TWT history, at least for the U.S., records that the early 1950s saw an appreciation of the thin, flat ladder as a practical periodic structure at millimeter wavelengths, provided one could invent a slow-wave interaction circuit incorporating it.[1,2] Reliable and inexpensive ladder fabrication by photo-etching a metal foil was envisioned, and so was fabrication by winding

wire or tape on a frame with the means used for preparing helices. However, as opposed to the helix turns, each ladder rung would be solidly anchored at its ends, mechanically and thermally; hence the permissible levels of beam and rf power might exceed those for a helix for comparable wavelengths. Also, if a glimpse into the future had been possible, the proposed ladder fabrication methods would have been hailed as obviating the accumulation of errors in the circuit period (as is common with fabrication by "axial stacking").

The first candidate ladder-based slow-wave circuit studied was a plain rectangular waveguide with the ladder simply installed in the broad wall, the rung span being quite a bit less than the waveguide breadth.[3] Slow-wave propagation was obtained here over a useful bandwidth (extending downward from the half-wave resonance frequency of a rung) which became greater yet when a ridge was introduced within the waveguide.[4] (The use of a shield over the ladder, outside the waveguide, was optional since wave slowing counterindicates radiation.) The propagation was "forward wave" and -- drawing on research from a later date -- the bandwidth depended on both the ridge-to-ladder capacitance and the space made available for loops of rf magnetic field to expand beyond the rung anchor points.

During the 1950s and beyond, and in various parts of the world, the single ridge plus thin, flat (or nearly flat) ladder combination appeared in low-voltage tubes -- primarily BWOs -- for frequencies up to 300 GHz.[5-7] In these designs, the disposition of metal around the rung anchor points varied,[8] hence the bandwidth contribution from this factor,[9] relative to that from the ladder-to-ridge capacitance, was not constant. Currently the interest in considerably higher power levels constrains the rungs to be anchored directly and at 90° to flat, solid walls[10] -- to maximize rung cooling. In this case, the bandwidth must be determined solely by the ridge capacitance. Coincidentally, most analytic efforts to model the structure's fields, impedances, etc., stipulated extensive flat walls normal to the array of rungs.[10-13]

Characteristic of the 1950s and early 1960s with regard to millimeter-wave tubes were beam voltages of at most a few kV (and rf power

levels so low that solid-state devices have since supplanted these tubes). To avoid an unreasonably fine ladder pitch it was natural to consider only space-harmonic interaction at these low beam velocities. (The beam-wave phase shift per period was between π and 2π for a BWO and 2π to 3π for an amplifier.) Thus, the first point made in H.G. Kosmahl's 1978 presentation[13] was that the tens-of-kV beam voltages favored today would permit non-space-harmonic operation at millimeter wavelengths of a "forward-wave" ladder-based amplifier with a relatively coarse pitch. Specifically, the suggestion of about $\pi/3$ phase shift per period at 21 kV would require only 30 ladder rungs per cm (77 per inch) at 42 GHz.

Of itself, "fundamental/forward" TWT interaction implies a relatively high rate of gain with distance, but Kosmahl's second point[13] was that the gain rate would also benefit from the high interaction impedance associated with the ladder. This impedance is due in part to the rung resonance at a frequency close to the operating frequency and the consequent high dispersion and low group velocities. Of course, a rather narrow "hot" bandwidth is associated with these circumstances, but Kosmahl's third point[13] was that many current applications might be satisfied with this narrow bandwidth if the TWA were inexpensive, short, easily focused and efficient due to the choice of interaction structure and the high gain per unit length.

In particular, a "hot" bandwidth in the vicinity of 1% was projected for the mid-band phase velocity of 0.267 c (c = 3E10 cm/sec) and group velocity of about 0.053c (with these values decreasing at the rates of 4.3% and 13%, respectively, per percent increase in frequency). This bandwidth prediction (at low beam perveances) is largely established by the angle of intersection between the ω-β curve and the "beam volocity" line on the Brillouin diagram. Because this angle is appreciable here, the frequency variation of the synchronism parameter will affect the "hot" bandwidth much more than the frequency variation of any other parameter (such as impedance). Any ω-β curve should therefore lead to about the same "hot" bandwidth if the phase and group velocities (and hence the intersection angle) are replicated.

2.3 CIRCUIT STUDIES FOR REFERENCE PURPOSES

Prior to devising and evaluating TWT designs that would both be practical and embody the principles presented above, some cold-test experimentation was undertaken with an intentionally simplified slow-wave structure. An objective here was to become familiar with and optimize the procedures for measuring dispersion and impedance, and to observe the effects of dimensional changes in a geometry featuring the basic structural elements -- rungs, ridge and side walls. In addition, interaction-impedance measurements might provide support for the high-impedance premise. Along with the dispersion curves obtained for various values of the geometric parameters, the impedance data would be supplied NASA-LeRC personnel for comparison with analytically projected values, testing the merit of new analytical techniques they had devised[13] and would be perfecting and extending in the future to the benefit of the microwave-circuits community.

Figure 1 describes the cold-test "reference" model constructed with dimensions providing a passband extending downward from about 3.2 GHz. (In this instance, any propagation possible at higher frequencies would not be of interest even if evidence of it had been observed.) The materials used were aluminum, copper and silver-plated brass, with silver-loaded lacquer applied to ensure contact at the various joints.

In the longitudinal view, the structure is eight periods long, as determined by short-circuiting "end plates" located so that the images of the ladder in these "mirrors" make it appear continuous and endless. In consequence, the structure should resonate electrically at eight frequencies within the passband, though some resonances closely spaced in frequency might not be separately resolvable in the presence of circuit attenuation. The dispersion curve is a plot of these frequencies vs the corresponding phase shift per period, $\theta = n\pi/8$ where $n = 1, 2, 3..., 8$. (To verify the value of n, the standing wave along the ladder can be identified from the perturbations in resonance frequency caused by a small metal bead traveling axially on a nylon thread.) To excite the structure electrically, small

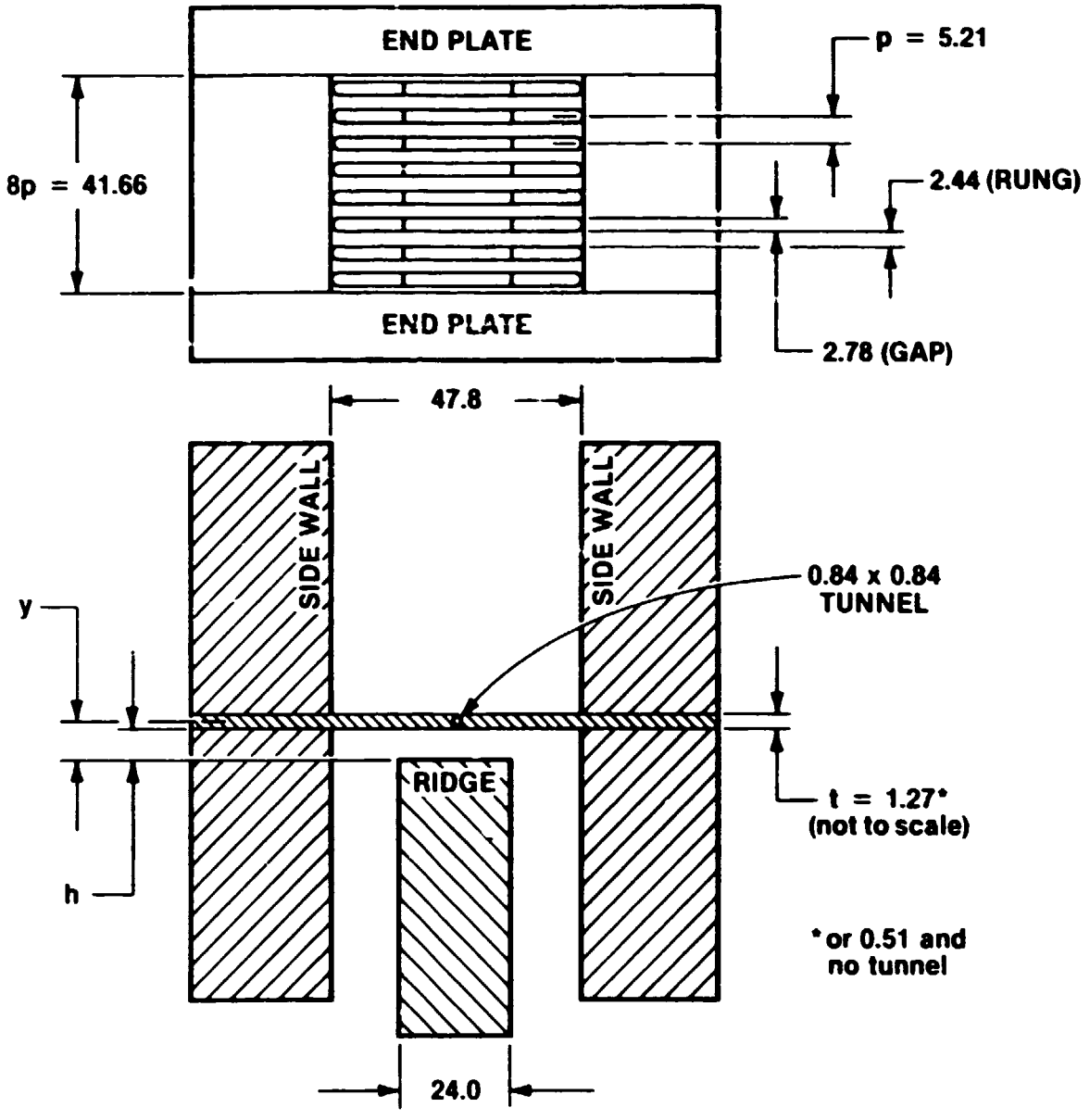

Figure 1. Essentials of eight-period cold-test model of basic forward-wave ladder circuit. (All dimensions in mm.)

coupling probes (E- or H- type or both) are inserted through tiny holes in the end plates provided for this purpose or for the passage of metal or dielectric "perturbers".

Referring to the transverse view (Figure 1), the sidewall spacing was maintained equal to the rung length which was constant along with the period, p, the gap-to-period ratio, and the ridge width. The variables were the ladder thickness, the ridge-to-ladder spacing, and the option of a second ridge, symmetrically disposed. The thicker of the two ladders used (1.27 mm or 0.050 inch thick) was able to have a small tunnel on the axis to accommodate a very slender sapphire rod (relative dielectric constant = 9.580 $\pm$ 0.27%), 0.831 mm (0.0327 inch) $\pm$ 0.15% in diameter. The percent downward shift in resonance frequency (100 $\Delta f/f$) due to the insertion of this rod is a measure of the interaction impedance on the axis (insofar as the rod is very thin and interacts negligibly with any tranverse E fields present).

Specifically, the "Kino impedance" is proportional to $\Delta f/f$ divided by the group velocity at f; the "Pierce impedance" is proportional to the Kino impedance divided by the square of $\beta = \theta/p$. Specifying impedances as "on the axis" does not imply that an electron beam might be provided there; in this instance the structure of Figure 1 is being characterized without any electron stream envisioned.

The data obtained were previously supplied NASA-LeRC in both graphic and tabular form (with resonance frequencies and percent frequency shifts stated with 5 and 4 significant figures, respectively) but only the graphs are reproduced here. Figures 2 and 3 show the effects of varying the ridge-to-ladder separation, for the single-ridge and double-ridge cases and the thicker of the two ladders available. It is clear that the greater the loading at the ladder center, the lower the dispersion. However, for the double-ridge case, the effect is less than for a single ridge positioned twice as close to the ladder.

When two ridges are used, they could serve as the conductors of a two-wire transmission line with the ladder lying ineffectually in an

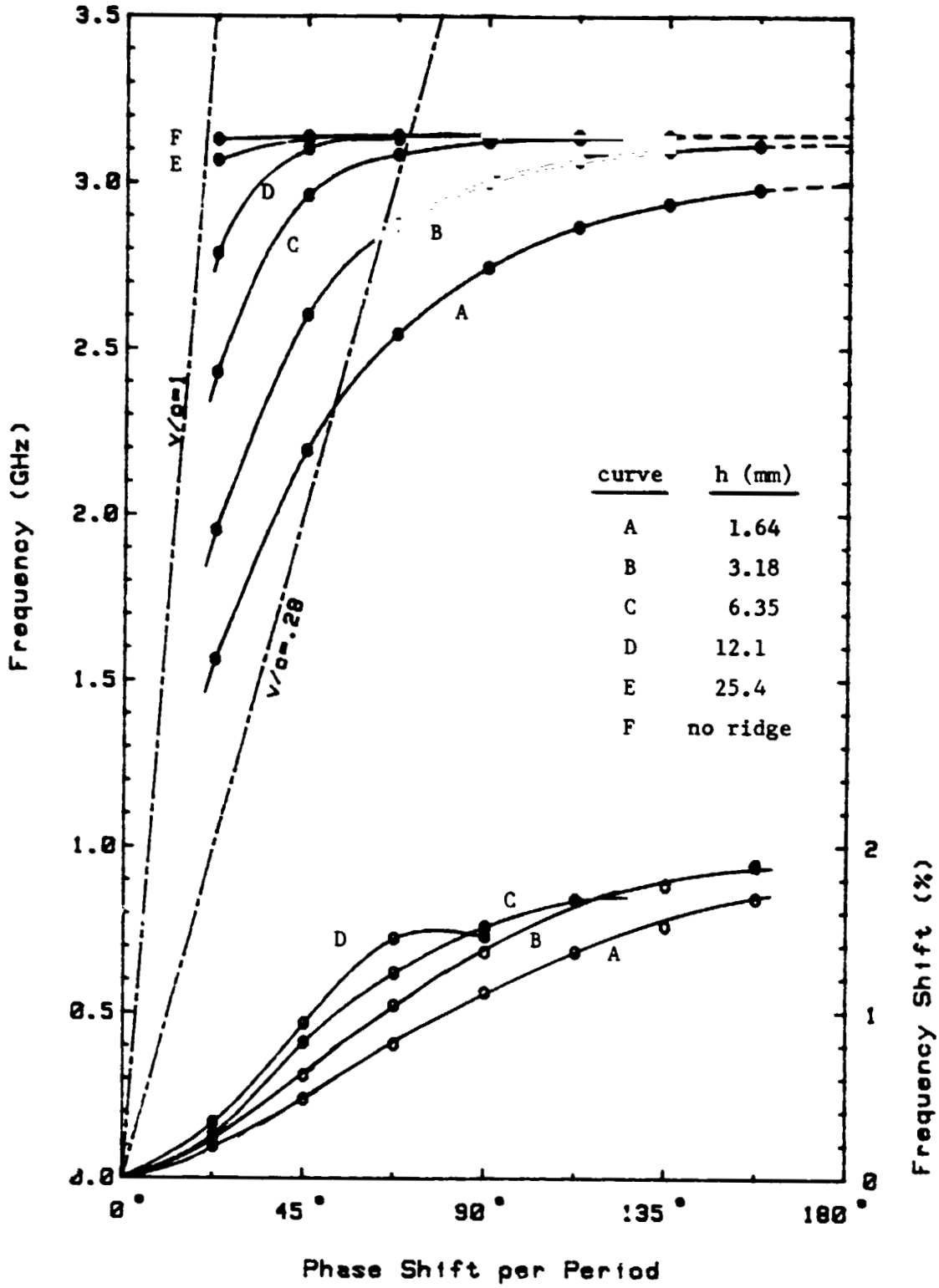

Figure 2. Dispersion and impedance measurement data for circuit model of Figure 1 with single ridge various distances from 1.27 mm ladder.

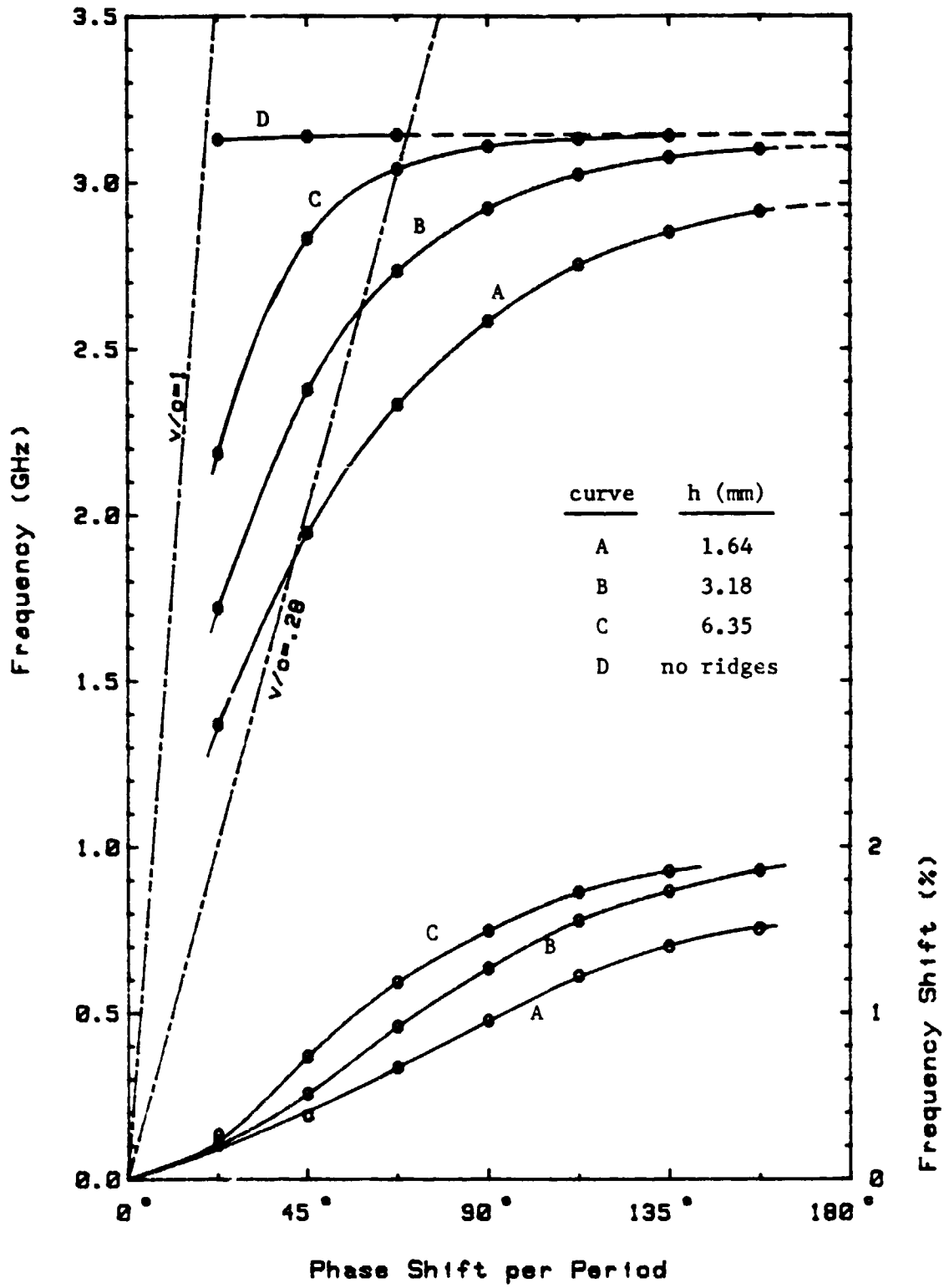

Figure 3. Dispersion and impedance measurement data for circuit model of Figure 1 with two symmetrical ridges and various spacings from 1.27 mm ladder.

equipotential plane. The dispersion curve for this extraneous TEM-mode "fast-wave" propagation would be the line v = c, with 3.6 GHz as the lowest possible resonance frequency for the model constructed. In addition to this frequency being beyond the range examined, the mode in question should not be excitable by the coupling probes used. This issue, along with others discussed in similar detail, may appear minor but will be seen to be relevant to the circuit studies covered in later sections.

While the thicker ladder was in the assembly, attempts were made to compare the sapphire-rod perturbations obtained using the central tunnel with those obtainable with the axial rod lying on one of the ladder surfaces, toward or away from the single ridge. The data supplied NASA-LeRC covered two values of θ for each of two values of ridge-to-ladder spacing, h, and were consistent with expectations regarding the degree of asymmetry produced by moving the ridge closer. However, interaction of the rod with transverse E fields would clearly be significant here making interpretation of the data problematic.

Figure 4 shows the effect of the ladder thickness for a constant ridge-to-ladder spacing -- for each of three values of this spacing. Since it is possible to define this spacing either on a surface-to-surface basis or on a surface-to-centerline basis, both interpretations were accounted for, where feasible, in preparing Figure 4.

Figure 5 shows the frequency dependence of K', a quantity proportional to the on-axis Pierce impedance, measured while varying the ridge-to-ladder capacitance and holding the rest of the geometry fixed (Figures 2 and 3). For a given resonance frequency f in GHz,

$$K' = K_1/K_2^2 K_3$$

where

K_1 = percent shift in resonance frequency upon insertion of specified sapphire rod;

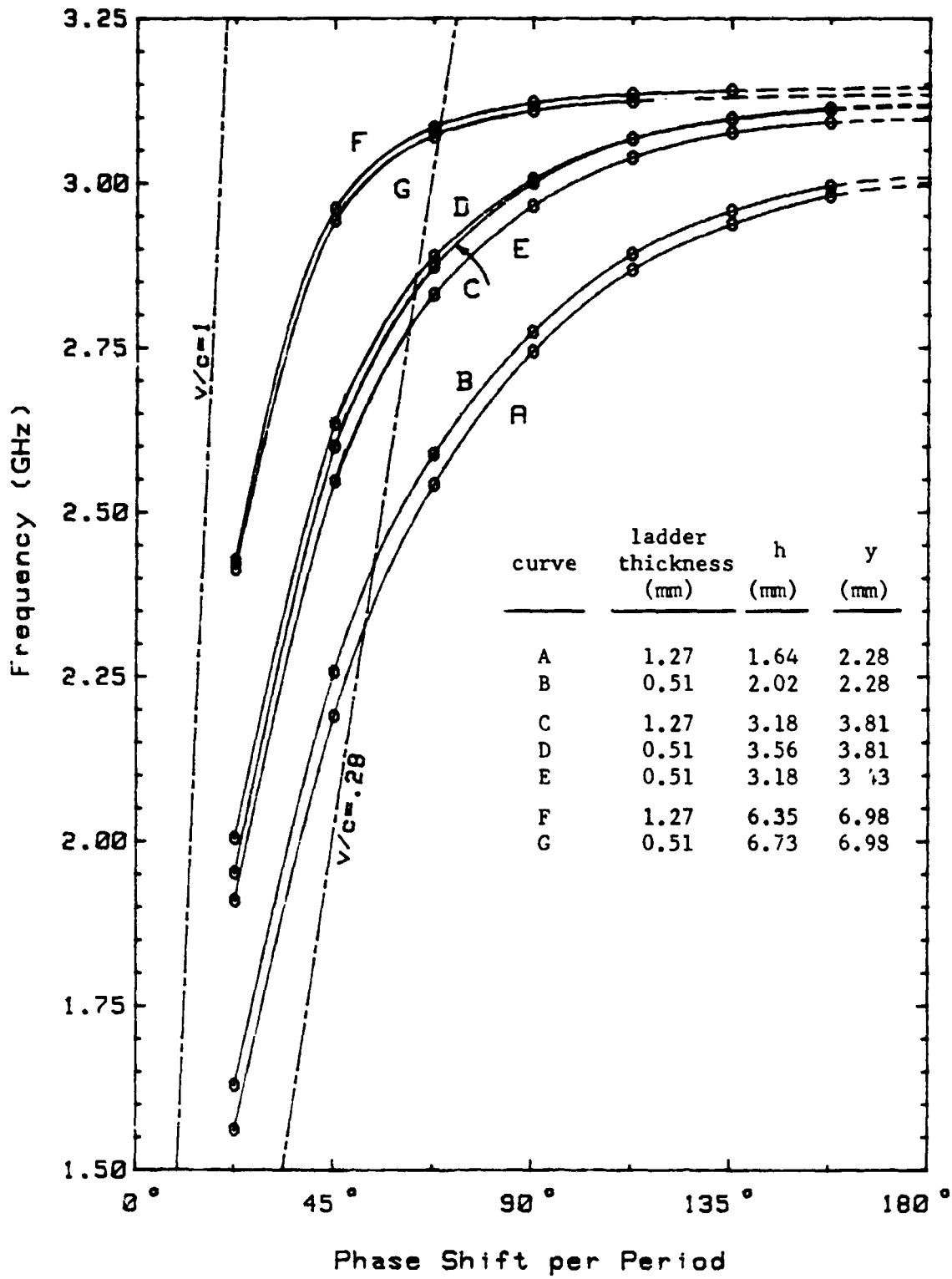

Figure 4. Dispersion data for model of Figure 1 with single ridge, 1.27 or 0.51 mm ladder thickness, and various distances from ridge to ladder surface or centerline.

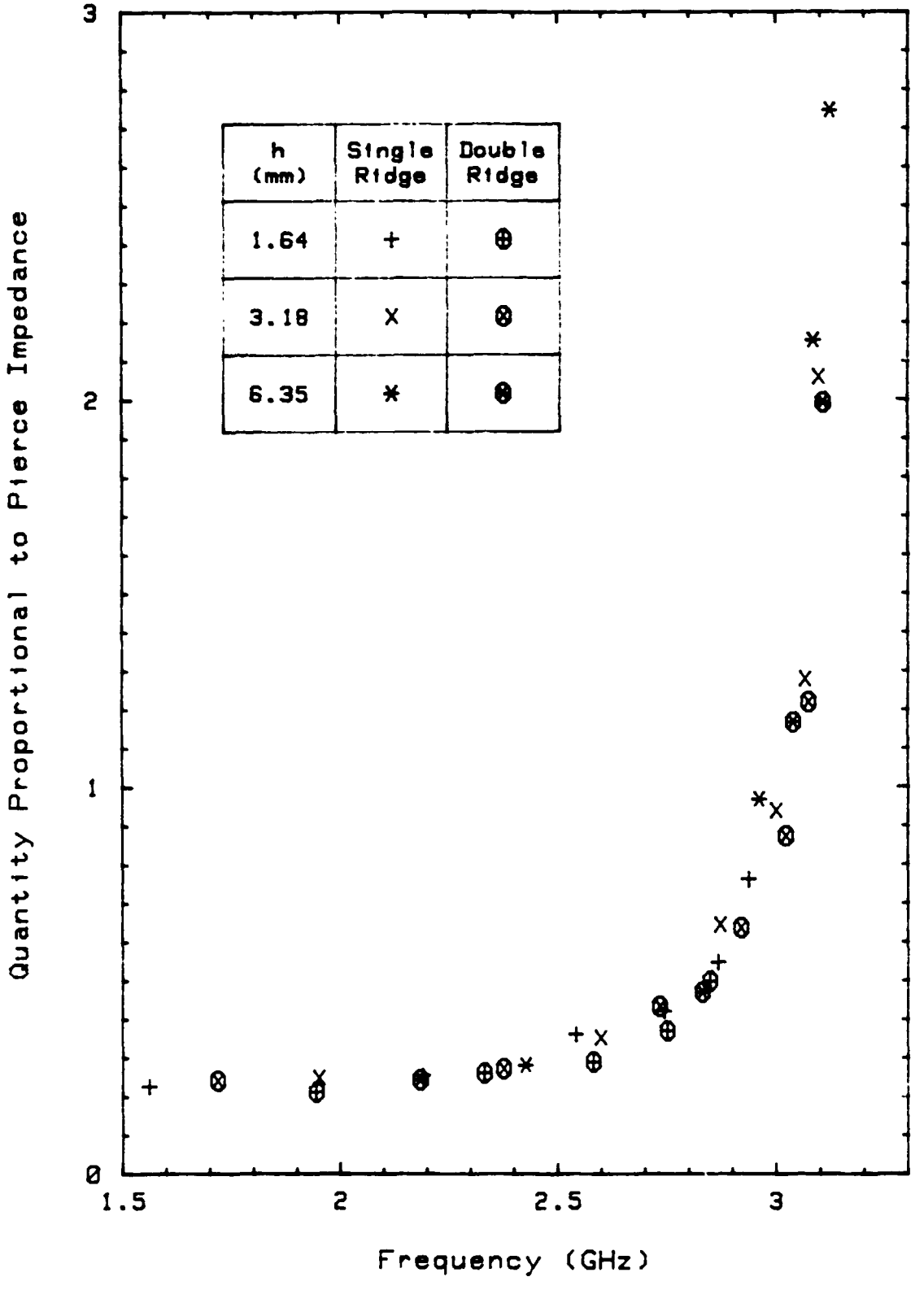

Figure 5. Impedance measurement data of Figures 2 and 3, for three ridge/ladder spacings, processed to show frequency dependence of Pierce impedance.

K_2 = radian phase shift per period in units of $\pi/8$; and

K_3 = graphically determined slope of dispersion curve, $\partial f/\partial K_2$, in those units.

Figure 5 suggests, for a thin, flat ladder geometry where only the ridge loading is changed, that the Pierce impedance is a function of the frequency alone, and not the number of ridges or their closeness to the ladder. However, it is to be noted that for a fixed frequency (a horizontal line in the upper portion of Figures 2 or 3), varying the ridge loading causes large changes in unit phase shift, $\theta = \beta p$, and in the synchronizing beam voltage. These factors should therefore be considered before drawing conclusions regarding gain and bandwidth from Figure 5.

2.4 PRACTICAL CONCERNS

Interaction-structure geometries differing little from that of Figure 1 were practical enough those many years ago[1,5-7] when the order of 10 ± 10 dBm of rf output power went along with beam power densities below 10 kW/cm^2. Such beams could be introduced as a flood of magnetically confined electrons (from non-convergent guns) with the only thermomechanical concern being the possibility of some rung buckling. (This was either prevented by winding tungsten tape under tension, or else allowed to occur for copper tapes pre-arched slightly in one direction.)

Today, an output-power requirement of 56 ± 3 dBm CW at 42 GHz creates a very different situation. Beam power densities of the order a few MW/cm^2 would be necessary and pencil-beam optics would be the only means for making this manageable from the viewpoints of both the gun and the interaction structure. On the interaction structure side, a low percentage interception is consistent with having a pencil beam in a round "tunnel" with a design filling factor not exceeding 67%. (The beam/circuit clearance in this circular case also represents less decrement of interaction impedance at the beam edge than would the same clearance in the planar case.) On the gun

side, the requisite 100 A/cm^2 or more of beam-current density is consistent with a conventional axisymmetric gun sufficiently convergent to avoid undue cathode loading.

Figure 6 depicts, in transverse section, an interaction-structure design proposed early in the contract to both capitalize on the electrical properties of the circuit of Figure 1, and accommodate a high-power pencil beam and the associated rf power levels. (The ladder period and rung dimensions in the longitudinal direction would be as shown at the top of Figure 1, assuming the same frequency-scaling factor.) The circuit of Figure 6 can be viewed either as two ladder/ridge combinations in parallel, or as one ladder with two ridges, said ladder being split into two halves separated at the center sufficiently to create a non-circular tunnel for the pencil beam. Another feature of this design is thermally conducting dielectric strips to support each ladder half relative to the adjacent ridge.

Electron-optically and thermomechanically, the tentative design of Figure 6 has several advantages which were retained after this design gave way to another. The unconventional tunnel cross-section should allow beam interception only at the ladder centers where the heat produced would be evacuated directly through the dielectric support rods which also fix the position of each rung in three dimensions. Given that the rf currents on a ladder rung increase from zero at the rung center to a maximum at each rung end, rf heating should be localized near the rung ends where cooling is provided by the ample side walls. In consequence of these considerations, the power-handling capability of the ladders shown should be considerable.

An appropriate cold-test model for this slow-wave-circuit design, scaled 16:1, was assembled and tested. A typical mapping of its propagation characteristics is reproduced in Figure 7. Since the ladder/ridge spacing here was 3.18 mm, and the dielectric had been omitted, it is not surprising that the lower ω-β curve in Figure 7 is close to the h = 3.18 mm ω-β curve of Figure 3. This illustrates that the ladder can be made non-planar with little change in electrical properties; in subsequent designs the deviation from planarity was made even greater.

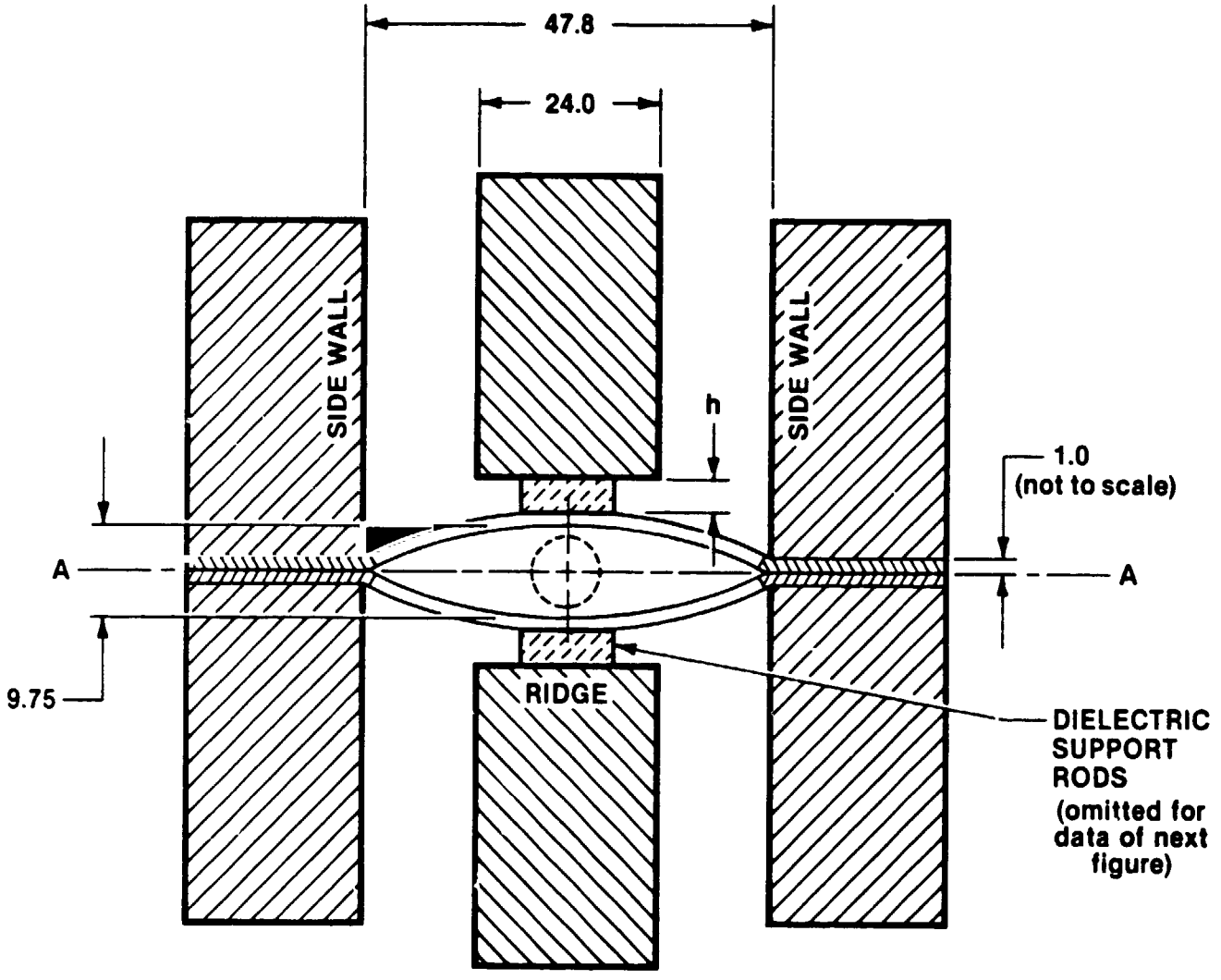

Figure 6. Essentials of double-ridge cold-test model with ladder of two layers arched apart at center. (Longitudinal section is same as at top of Figure 1; all dimensions in mm.)

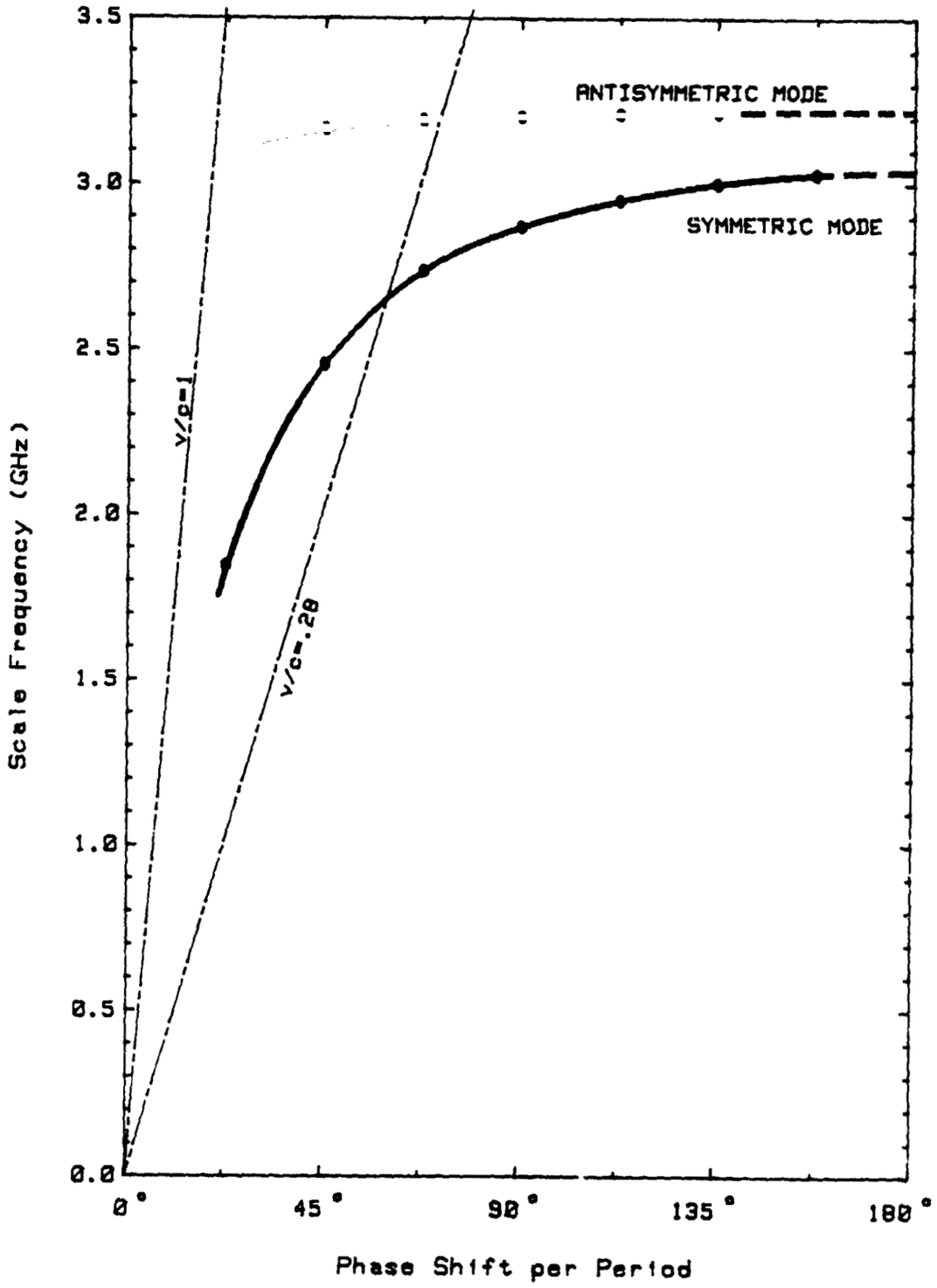

Figure 7. Dispersion curves for two modes of circuit model of Figure 6 at ridge/ladder spacing of 3.18 mm.

Another very important point to be made by including Figures 6 and 7 here concerns the antisymmetric mode of propagation not previously manifested. Its ω-β characteristic is the upper one in Figure 7. Since the longitudinal E field, E_z, is zero on the axis for this mode, it would not usually be a useful mode. However, interaction is certainly possible with a finite-diameter beam, and when the two ω-β curves are as close as they are in Figure 7, the likelihood of impaired TWT performance is considerable. (No possiblity of differential loss loading exists here, nor is it likely that the input/output end couplers for the circuit could easily be designed so as to defeat net gain for the antisymmetric mode without adversely affecting the symmetric mode.)

Since both modes are able to propagate in the interaction-structure designs studied hereafter, a review of the mode distinctions is in order: For the wanted symmetric (or even) mode, each ridge and ladder has the same rf potential as its opposite member in a given transverse plane. On the axis, E_z is finite though somewhat reduced from its strength at the ladder surface. For the problematic antisymmetric (or odd) mode, each ridge or ladder is in rf antiphase with its opposite member, consistent with transverse E-field lines crossing the midplane (A-A in Figure 6). As for E_z, it is zero not only on the axis but everywhere in midplane A-A. All the properties of this mode can thus be accounted for most readily by imagining plane A-A as a conducting surface, with the circuitry below A-A serving merely as the electrical image of that above. It would then follow that the two ω-β curves will differ, but not by very much, in the case of Figure 6.

2.5 PROPOSED CIRCUIT DESIGN

The entire body of ideas reviewed above was utilized in arriving at the proposed 42 GHz "TunneLadder" interaction-structure geometry described by Figure 8. Two ridges and a single ladder, assembled from two identical components, continue to be evident. The shaping of the ladder halves provides a quasi-elliptical beam tunnel so that beam interception will occur predominantly at the two positions where heat can travel directly outward through the dielectric support rods. Moreover, the new ladder-half shaping

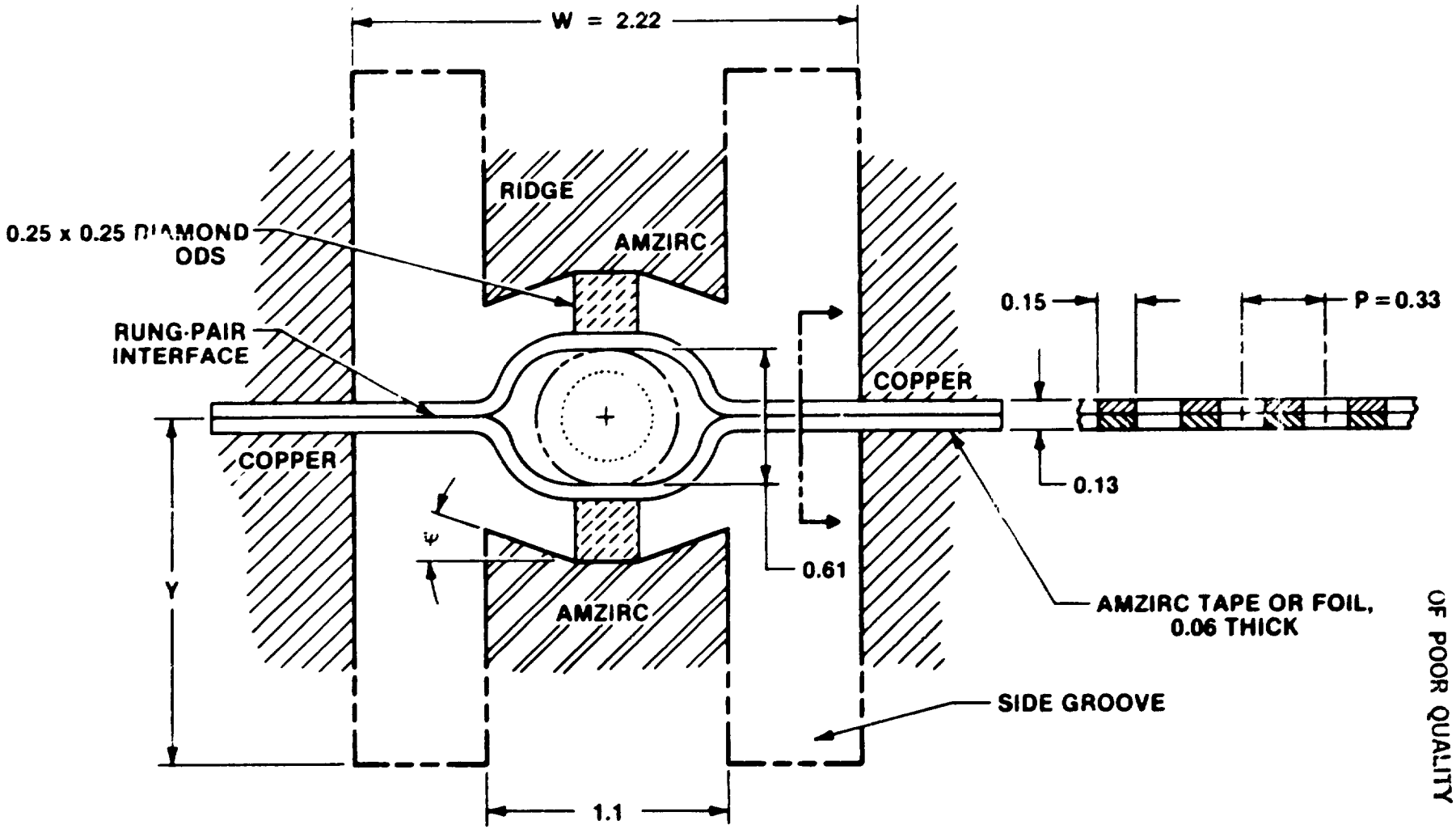

Figure 8. Essentials of proposed "TunneLadder" interaction structure for narrow-band millimeter-wave power TWT. (All dimensions in mm for 42 GHz operating frequency; circles show nominal beam and tunnel diameters.)

results in a large increase in the frequency at which antisymmetric-mode interaction might be possible. Specifically, the ratio of this frequency to the symmetric-mode operating frequency roughly equals the ratio of the total rung length to half the circumference of the quasi-elliptical tunnel. Experimental data for the two modes are covered in Section 4.3. Additionally, insofar as the tunnel or "eye" is small compared with the rung length, the azimuthal variation of E_z at the beam edge will be minimal for the symmetric mode.

Figure 8 also indicates the proposal of Type IIA diamond rods, nominally 0.25 mm square in cross-section, as support rods of high thermal conductivity running the full length of the circuit structure. The copper of the ladder rungs and ridges would be zirconium doped to effect strong thermocompression bonds to the diamond rods without the risk of contaminating the exposed diamond surfaces. Further details relating to these rods and the bonding are discussed in Chapter 3. As noted previously, rf heating of the ladder rungs is rather well separated spatially from the beam-interception heating, with the rf-dissipation heat flowing for the most part directly to the side walls. The confirmatory results of a quantitative thermal analysis are reviewed in Chapter 7.

2.6 "TUNNELADDER" TWT VS MILLIMETER-WAVE HELIX TWT

Since the proposed amplifier is based on non-space-harmonic interaction, a forward-wave circuit, and a round beam tunnel, comparison is invited with a helix-TWT design for the same frequency region. The major differences appear to focus on the reduced bandwidth and accompanying increased interaction impedance in the TunneLadder case. Specific comparison will be made with a particular millimeter-wave helix-TWT design[14] being developed at Varian under the direction of A. Jacquez (Figure 9). In fact, the beam-tunnel diameter, beam filling factor, diamond-rod dimensions

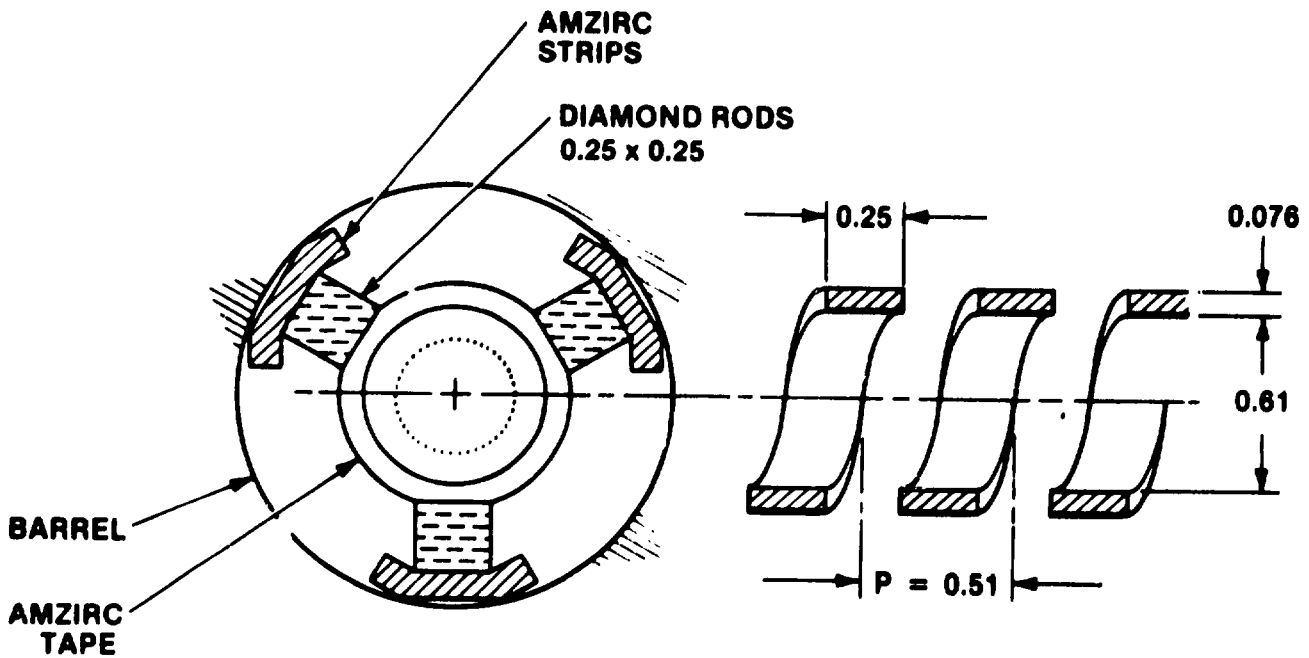

Figure 9. Essentials of Varian helix-TWT design for 20 to 40 GHz. (Contract F33615-79-C-1737).

and Amzirc/diamond bonding technology applying to Figure 8 were taken at the outset from Figure 9 (drawn here to the same scale). The angled contour of the ridge surface facing the ladder in Figure 8 serves to position the diamond rod with less risk of stressing the bonded diamond than a straight-sided groove might entail; the idea was taken from the shape of the copper strips interposed between rods and barrel in Figure 9.

Further points of comparison relating to design decisions may be listed as follows:

Parameter or Feature	Helix TWT (Figure 9)	"TunneLadder" TWT (Figure 8)
Operating frequency (GHz)	20 to 40	42 (1% bandwidth)
Beam tunnel diam. (mm)	0.61	0.61
Nominal beam diam. (mm)	0.41	0.41
Beam voltage (kV)	10	21
Microperveance	0.2	0.06
Beam current (mA)	200	180
Beam power (kW)	2.0	3.8
Min. desired rf output power (W, CW)	100	200
Brillouin field (gauss)	1840	1460
Tape size (μm)	76 x 254	64 x 152
Periodicity (turns/cm)	20	30
Support system	3 diamond rods around circle	2 diamond rods at center of tapes, anchored to side walls at ends
Interception heating	uniform around circle	localized near center of tapes
RF-dissipation heating	uniform around circle	mostly near anchored ends of tapes

Additional points of comparison relating to inherent properties of the two slow-wave structures are as follows. The justification for some of these statements is made in later sections of this report.

Item	Helix	"TunneLadder"
Relative interaction impedance on axis; gain/unit length	low	high
Relative tube length	long	short
Relative copper losses	high	low
Relative rf electric fields; potential dielectric losses	low	high
Relative sensitivity to dimensional deviations	low	high

With regard to stability, π-point oscillation needs to be considered in the helix TWT, with a "velocity step" planned for suppression purposes. Stability concerns in the TunneLadder case relate to two extraneous modes of slow-wave propagation: the aforementioned antisymmetric ladder mode and another mode (see later) with a passband at yet higher frequencies. Provided the potential beam-interaction frequencies for these modes are very high relative to the operating frequency, the likelihood of oscillation is remote.

Both the helix and TunneLadder structures permit a TE "fast" wave to propagate along them at the signal frequency. Electronic interaction cannot occur, but if conversion of signal power to this mode takes place, the converted power can feed back toward the input and sustain oscillation upon reconversion. In the helix case, it is the "barrel" that supports a TE^{o}_{11} wave as if the helix were almost transparent, and it is primarily the radial input/output connecting wire at a helix end that converts a small amount of signal power to this mode. However, the resistive coating normally applied to dielectric support rods to effect a "sever" for the helix slow wave is also an adequate absorber of fast-wave power.

In the TunneLadder case, the two ridges support a TEM wave as if they were the conductors of a two-wire transmission line and the ladder were essentially transparent. (This applies at the operating frequency which is well below the frequencies at which this mode turns into the slow-wave antisymmetric ladder mode.) Conversion to this mode from the symmetric slow-wave ladder mode would be caused by asymmetrical imperfections on the

circuit or in the end transitions to waveguide. The converted wave might be cancelled dynamically by mechanically adjusting asymmetric counterbalances in the end couplers, or else absorbed by the resistive coating on the dielectric support rods that also provides a "sever" for the ladder slow wave.

2.7 RELATION TO OTHER PUBLISHED DESIGNS

Although the slow-wave circuit of Figure 8 is not fabricated with rings, the structure does effectively contain a series of rings, spaced along the axis. These rings are not interconnected by a single axial connection, as in the "ring-bar" circuit, nor by the two axial connections of Crepeau and Itzkan's circuit.[15] Neither are the rings supported by two flat fins as in the "ring-plane" circuit.[16] However, the "ring-plane" reference work[16] does consider the possiblity of slitting each "plane" to form a comb[17] such that the topology of Figure 8 is fairly well reproduced, (with the option of additional ridge loading[18]). Actually, using the notation established for ring-based structures, the TunneLadder circuit can be viewed as a "ring-stub" circuit, with ridge loading. In any event, the existence of pairs of propagating modes, corresponding to the ring halves being in phase or anti-phase, is amply focused on in the references cited.

The most advanced use of the ring-stub structure, with ridge loading, was undertaken at Thomson-CSF.[19,20] The essentials of the circuit design are shown in Figure 10. The proportions of the rings and stubs here are such that the symmetric and antisymmetric modes of propagation are very close in - space, hence the addition of a pair of "straps" per period to at least raise the passband frequencies of the antisymmetric mode with little change for the symmetric mode. (There would be no antisymmetric mode only if it were possible for the straps to have zero inductance, so the ridges would have to be at the same rf potential.) Referring to the design of Figure 8, the addition of ridge-to-ridge strapping (through the spaces between ladder rungs) would be inconceivable at millimeter wavelengths. Conveniently, the geometry shown for the TunneLadder structure of itself results in a ratio of about 2:1 between the possible interaction frequencies for the extraneous and the useful modes.

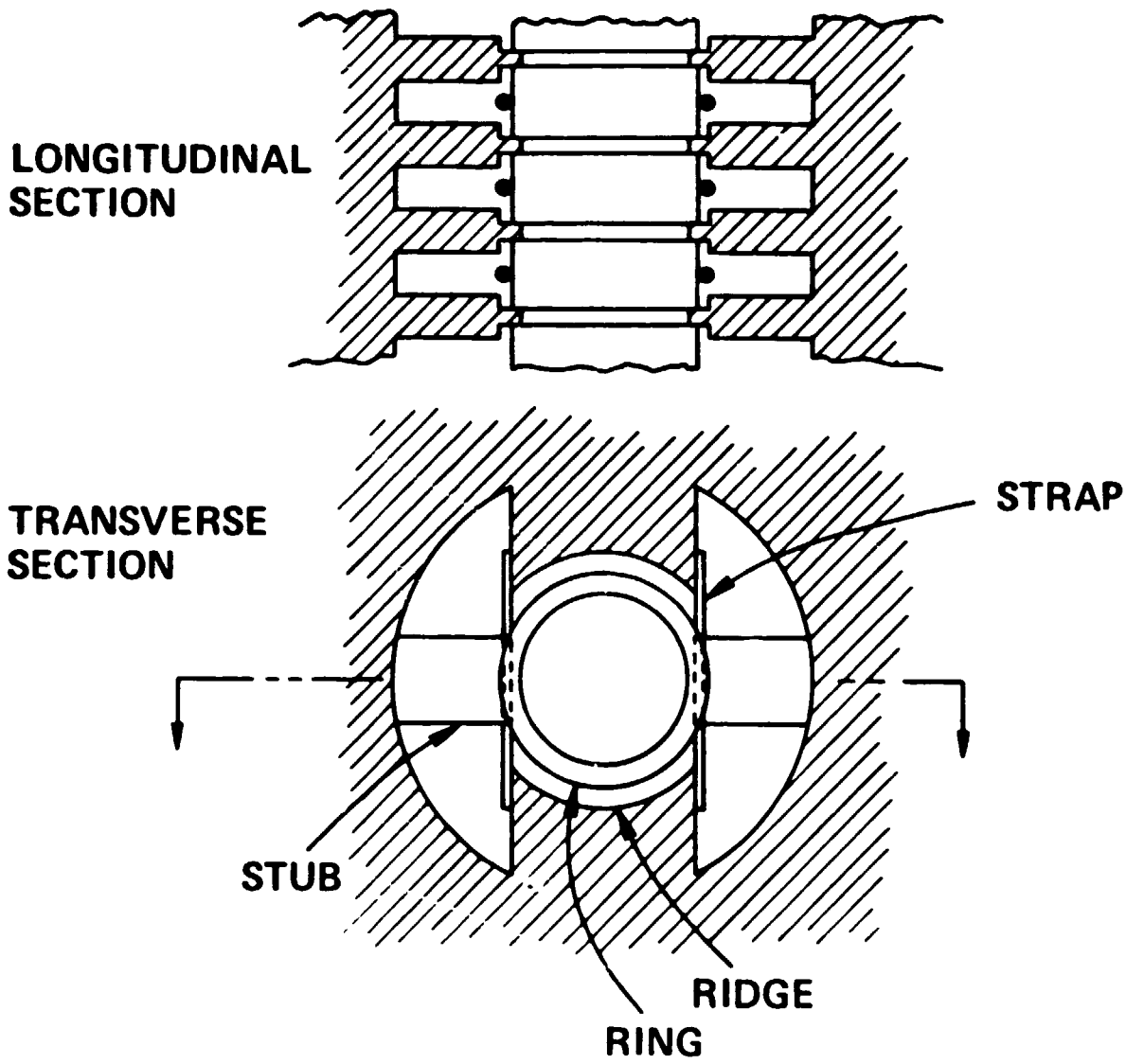

Figure 10. "Forward/Fundamental" TWT structure based on ridge-loaded, stub-supported rings, used at Thomson-CSF at C-band c. 1962 and at S-band c. 1974.

3.0 DIELECTRIC SUPPORT RODS

The dielectric support rods of the "TunneLadder" TWT circuit design (Figure 8) have discussion priority. The choice of properties and dimensions for these rods in the present context is so limited that the selection must be made at the outset and thereafter set the limits on what might be achieved, mechanically and electrically, for the circuit as a whole.

In common with the millimeter-wave helix-TWT design[14] (Figure 9), Type II A non-synthetic gem-quality diamond is selected for its exceptionally high thermal conductivity -- the better to evacuate heat due to even a low percentage interception of the 3.8 kW of beam power. This thermal conductivity is subject to variation with impurity content (nitrogen) of the natural diamond, but for engineering purposes the data of the uppermost curve in Figure 11 have been adopted, with possible anisotropy neglected. This figure allows Type II A diamond to be compared with Type I and with other candidate support-rod dielectrics. Unlike metals, the thermal conductivity of these dielectrics decreases pronouncedly with increasing temperature.

The square cross-section 0.25 x 0.25 mm is a standard size within the range that might suit the circuit for the frequency of interest. A recommended length is 2.5 mm, but greater lengths up to perhaps 5 mm are also available from the supplier. To minimize the electrical and thermal effects of anisotropy, an order of rods would be obtained with the same crystalline orientation. Even so, the total cost would be a small part of the total TWT production expense. As shipped, two of the 0.25 x 2.5 mm surfaces are polished and the other two cleaved, with a tolerance of ± 0.025 mm on the 0.25 mm dimension. Consequently, all of the group of rods needed for one tube would have to be selected out of a larger batch to reduce the tolerance range. After this, lapping of the rods in this group on at least three of the long faces would probably be necessary to obtain still less dimensional variation.

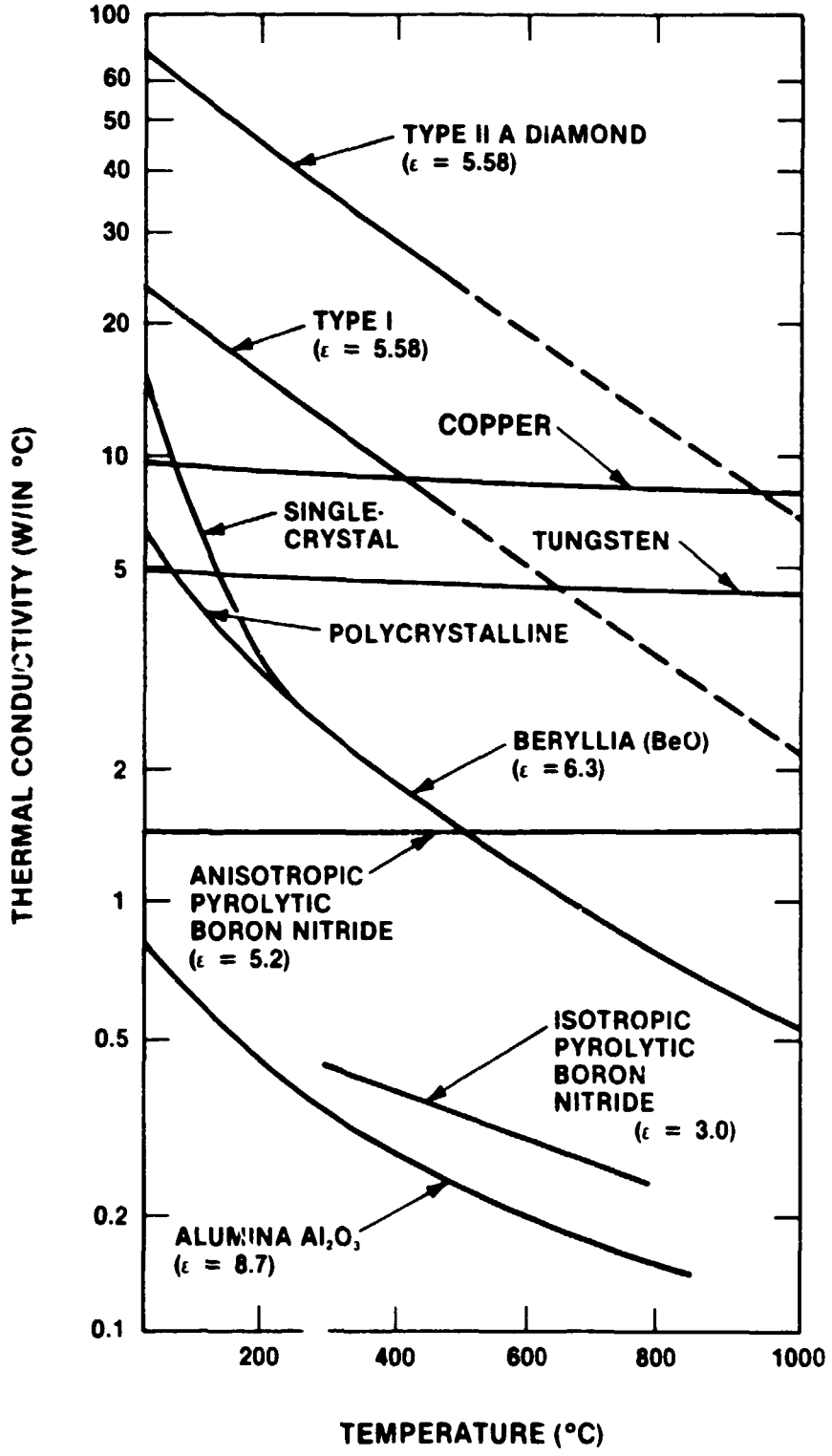

Figure 11. Temperature dependence of thermal conductivities of various support-rod dielectrics and associated metals.

To cover the full length of the TWT circuit (very likely including a "sever") a number on the order of ten of the short diamond rods would be laid end to end along each ridge. After bonding to the ridge, one long rod would result, but consideration might have to be given to whether the interface between consecutive rodlets should fall under a ladder rung or between rungs. Should this interface constitute an electrical discontinuity, consideration would have to be given to minimizing the overall electrical disturbance at the frequency of interest through the ratio of the rodlet length to the circuit period, or through specifying random rodlet lengths. Since such reflection-reducing schemes are valid only for passive circuits, it is fortunate that the potential discontinuity is avoidable by preventing any gap from opening between consecutive rodlets at the circuit operating temperature. That is, if the rodlets are just touching when bonding to the ridge is implemented at 1030°C, they will remain touching (and under some axial compression due to copper's higher thermal expansion coefficient) at any lower temperature.

Bonding of diamond to copper (tapes on one side, solid on the other) is accomplished at Varian by having the copper doped with zirconium (the alloy Amzirc) as the activator while heat and pressure are applied in a suitably inert atmosphere.[14] Such bonds are 100% reliable and stronger than copper or diamond, and the thermal resistance of the bonding interface is negligible. Moreover, all diamond surfaces not bonded to Amzirc are free of contaminant deposits. This is essential to minimize rf losses and rf breakdown problems. (Amzirc is harder than copper but the thermal and electrical properties differ very little.)

The value 5.58 is the currently accepted relative dielectric constant for diamond for the frequencies of interest. No documentation has been found regarding either the applicable dielectric loss tangent or the rf breakdown strength along a diamond surface. Both are more important in the TunneLadder-TWT case than the helix-TWT case (Section 2.6) because of much stronger rf fields for a given rf power level. Hopefully, as a result of directed research undertaken in the near future, the properties at 42 GHz and tube temperature of Type IIA diamond -- that has been heated in helium to 1030°C -- will be found as excellent as is presently expected.

In May 1979 (i.e., prior to the appearance of the book edited by Field[21]) a computerized literature search was undertaken, covering the previous ten or more years. Science Abstracts (copyright I.E.E.) and Chemical Abstracts (copyright Am. Chem. Soc.) were interrogated with descriptors such as: diamond, thermal conductivity, dielectric constant, and dielectric loss. Quite a few responses were printed out, mainly under CAS Registry No. 7782-40-3. However, the emphasis was too often on low temperatures, optical wavelengths, synthetic diamond, and only theoretical predictions of the electrical parameters sought. The printouts were saved, hence future work might include an update and more detailed review of this search to better uncover possibly pertinent information. A bibliography of unclassified reports is also on hand, obtained in May 1979 from the Defense Documentation Center (Search Control No. 083222) using the "first-level search terms" beryllia, beryllium oxides and diamond.

Apart from diamond, beryllia (ceramic) is a possiblity for the dielectric support rods if an order-of-magnitude lower thermal conductivity (Figure 11) might be tolerated. This low-loss insulator is well characterized electrically and the rods would be obtainable full-length and of any desired cross-sectional dimension. The bonding of Amzirc to beryllia has also been found to be as successful as for diamond, using the same procedures.

Single-crystal beryllia, as opposed to ceramic or polycrystalline, was also considered because of the promise of a thermal conductivity above that of ceramic BeO, though below that of even Type I diamond. However, the improvement is significant only below 150°C and nonexistent above 500°K (227°C)[22]. Nevertheless, if available, it might be preferred to ceramic BeO, despite circuit temperatures above 300°C, if evidence existed for lower dielectric losses. (The best rf use of single-crystal BeO might be in waveguide windows where the size precludes diamond but where temperatures below 150° might prevail).

4.0 TUNNELADDER SCALE MODEL AND COLD-TEST RESULTS

4.1 FIRST PHASE

Figure 12 shows the eight-period slow-wave circuit model, scaled 16:1, used to finalize the design geometry and, while doing so, obtain important data regarding eventual performance. Although the ladder period and rung profiles could not be altered, the sidewall-to-sidewall distance, identified as W (and also equal to the overall rung length projected onto a horizontal plane), was varied and the effects on propagation documented. Changing the details of the ridges was similarly investigated. Implicit in this documentation are indications of performance sensitivity to dimensional deviations. Insertion on the axis of a standardized sapphire rod (in this case of diameter 2.573 mm and relative dielectric constant 9.490) provided the resonance-frequency shifts from which interaction impedance was deduced.

The model of Figure 12 reflects the design choices indicated in Figure 8 except for the specific shape of the tunnel. However, the approximation is adequate at this stage of development. The light squares bracing the rung centers in Figure 12 are the ends of dielectric rods simulating the eventual diamond support rods (enlarged 16:1). The material used was Emerson and Cumming Stycast hi-K with K = 5.0 $\pm$ 3%, hence the deviation from diamond's K = 5.58 might be as much as 13%. Greater design refinement in the future would require a special order of Stycast better matching diamond in dielectric constant.

For the initial studies, the Stycast rods were absent and the ridge surfaces facing the ladder were simply flat. The ridges and sidewalls were then adjusted until the measured ω-β curve (for the symmetric ladder mode) was about as desired. This desired curve should pass through the point $\theta = 60^{\circ}$, F = 2.6 GHz (approximately) and have about the same slope (group velocity) as the curves for h = 3.18 mm in Figures 3 and 7. Accordingly, W = 38.6 mm and h = 1.78 mm (less than the W and h of Figures 1 and 6 that provided the indicated curves in Figures 3 and 7 respectively) were required for the new shaped-ladder model, where h is always defined as the surface-to-surface ridge-to-ladder spacing. (The non-critical ridge width in this

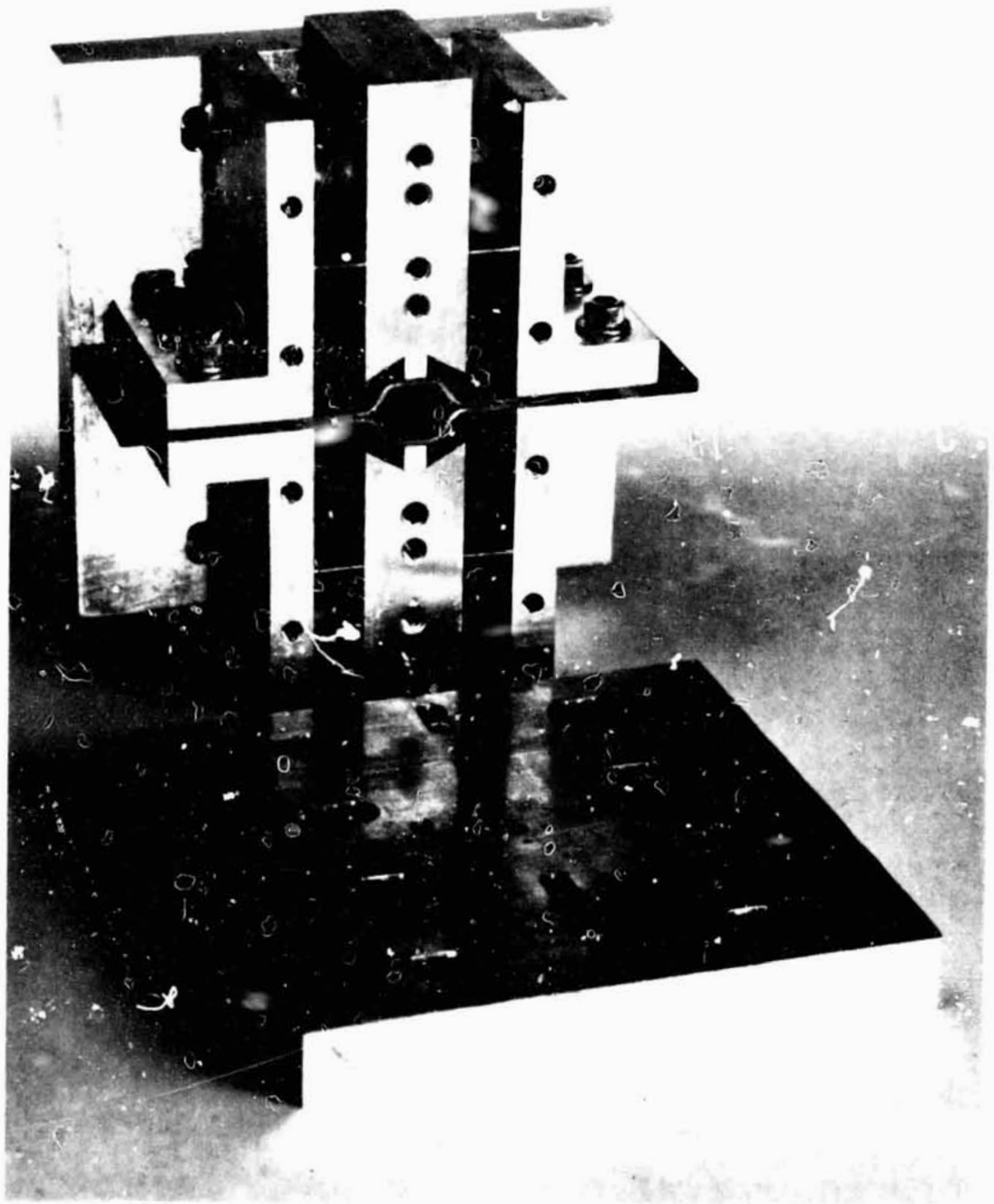

Figure 12. Eight-period "TunneLadder" cold-test model built to 16:1 scale.

case was 19 mm.) The actual ω-β curve and the sapphire-rod perturbation results are recorded as curve A in Figure 13.

The initial rise of Δf/f (indicator of interaction impedance on the axis) in a curve at the bottom in Figure 13 reflects the rapid increase with frequency of the impedance in the rung plane (Figure 5) while at low β (many periods per wavelength) the rung-to-rung E fields extend readily to the system axis. The subsequent falloff in Δf/f indicates the strong effect of increasing β (fewer periods per wavelength) in raising the decay rate of the ladder's axial E fields, going from the rungs to the system axis. The Δf/f magnitudes for Case A (Figure 13) are the largest obtainable with this model since dielectric has not yet been introduced outside the tunnel, with its tendency to weaken fields inside.

4.2 SECOND PHASE

When the square-section dielectric rods (4.06 x 4.06 mm Stycast in the large-scale model) were finally introduced in the cold-test model, conforming to Figures 8 and 12, all experimental evidence indicated that the ridge-to-rung capacitance was now being provided entirely by the dielectric. This capacitance could therefore be viewed as lumped, and the sensitivity of the ω-β curve to capacitance deviations (resulting from changes in rod material or dimensions) would be predictable from the data of Figure 3. That is, the sensitivity (of curve B in Figure 3) to a given percentage change in the air-gap spacing, and the sensitivity to the same percentage change in the substituting lumped capacitance, should be about equal.

When the dielectric rods were introduced it was necessary to decrease the sidewall separation, W, since the dielectric added some incidental rung-to-rung capacitance while providing for the rung-to-ridge capacitance. The sensitivity to deviation from the adopted W may be noted from Figure 13. The difference between ω-β curves C and D -- a frequency shift of about 3 or 4% -- is entirely due to a change in W of 3.4%, suggesting a 1:1 correspondence. The angle ψ (Figure 8) was varied from 0 to 20° with W = 34.3 mm and from 20 to 30° with W = 35.5 mm. The minimal electrical consequences of

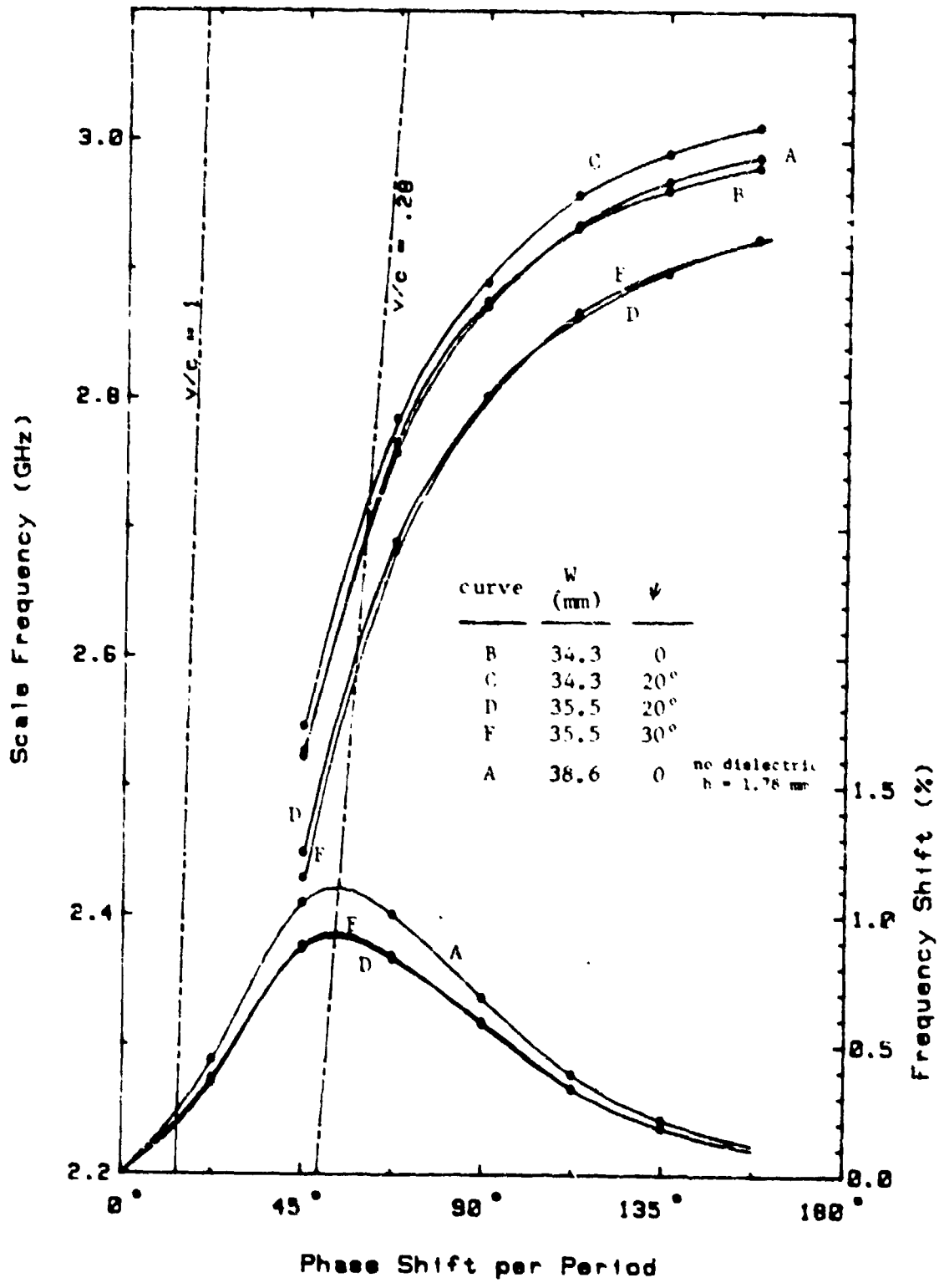

Figure 13 Dispersion and impedance measurement data for circuit model of Figure 12 with various small geometric changes implemented

these variations indicate how little sensitivity there is to the angle ψ, which would therefore be chosen only as mechanically convenient. (The purpose of this design feature is merely to center the dielectric rod. In Figure 13, the apparently paradoxical location of curve C relative to curve B may reflect dimensional fluctuations between successive model reassemblies.) This electrical indifference to the ridge shape following installation of the dielectric rods reinforces the conclusion that the dielectric insert becomes essentially the sole determinant of the ridge-to-ladder capacitance.

4.3 COMPLETE MODE PICTURE OF FINAL CIRCUIT DESIGN

4.3.1 Symmetric Ladder Mode

Figure 14 documents the three lowest-order modes of propagation for the finalized interaction structure. These data were readily obtained with the resonated eight-period model of Figure 12, given the choice available of excitation probes and holes for their insertion. The lowermost curve (same as E in Figure 13) represents, of course, the symmetrical ladder mode which would provide for the useful gain of the proposed TWT. The intersection of this curve with the diagonal line representing the slow space-charge wave (of a 21 kV electron beam) should correspond to the (scaled) operating frequency and the desired phase shift per period. The quite narrow "hot" bandwidth centered at this frequency is also suggested. Where the ω-β curve tends to be horizontal, propagation is termed rather "slow-wave", with low phase and group velocities and increased circuit attenuation. Axial E fields are relatively strong, but only near the tapes, not near the axis, for these higher values of β. Where the ω-β curve tends to be vertical, relatively "fast-wave" propagation is indicated, with low circuit losses but also very little axial E-field strength. (The issue of a lower cutoff frequency other than zero for the symmetric ladder mode is taken up later.)

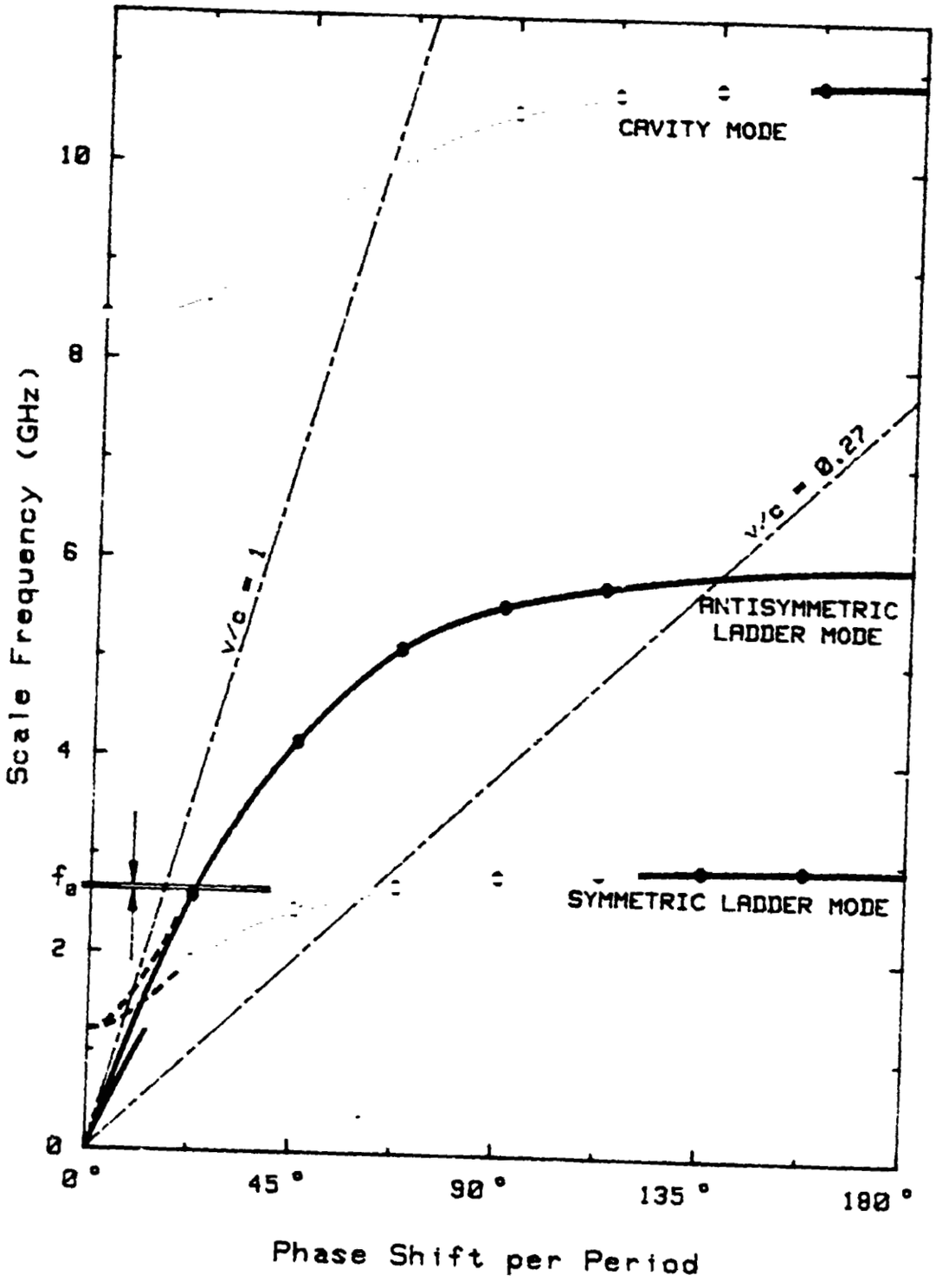

Figure 14. Dispersion characteristics for three lowest-order modes of final "Tunne-Ladder" interaction structure. (W = 35.5 mm; ψ = 30°.)

4.3.2 Antisymmetric Ladder Mode

The antisymmetric ladder mode (Figure 14), previously discussed with reference to the structure of Figure 6 (see also Figure 7), now propagates at much higher frequencies since the effective rung span for this mode is only about half that for the symmetric mode. (Antisymmetric-mode properties are consistent with the notion of a conducting surface lying in the ladder mid-plane, with zero axial E fields everywhere in this plane.) Accordingly, electrons in some parts of the beam cross-section (those close to the support rods) could interact with the fields of this mode, permit forward-wave gain, and allow oscillation if that gain exceeded the total losses of the likely feedback path. However, the frequency (about 5.8 GHz in Figure 14) would be over twice the operating frequency and the reduced skin depth, and the very low group velocity at $\theta = 133^{\circ}$, suggest high circuit attenuation. Moreover, the large value of θ signifies very weak axial E fields along all electron trajectories except those grazing the rungs (and near the support rods). In sum, the risk of oscillation in this regime is minimal.

As further insurance, it might be feasible to introduce an intentional "contact resistance" where two rungs rest against one another to form a pair (see "rung-pair interface" in Figure 8). This resistance would affect neither the symmetric ladder mode nor the thermal properties of the structure. (The rung-pair interface is a Dirichlet boundary for the antisymmetric ladder mode but a Neumann boundary for the symmetric mode and for the thermal system.) However, circuit attenuation should increase for the antisymmetric mode at frequencies where it is "slow-wave" and perhaps also at the lower frequencies where it is "fast-wave". As discussed in Section 2.6, there is a problem of possible feedback at the operating signal frequency (2.6 GHz in Figure 14) through accidental conversion of power from the symmetric mode ("slow-wave" at 2.6 GHz) to the antisymmetric mode ("fast-wave" at 2.6 GHz) and added loss for the antisymmetric mode alone could be beneficial. As discussed in a later section, no portion of the proposed interaction structure is utilizable for adding loss differentially for the unwanted mode -- with the exception of the rung-pair interface.

The issue of a lower cutoff frequency other than zero for the anti-symmetric ladder mode, as well as for the symmetric mode, is taken up later. In any event, the lower cutoff frequency must be the same for both ladder modes.

4.3.3 Cavity Mode

Figure 14 also documents the propagation characteristic of a third or "cavity" mode with a very high-frequency passband of 8.4 to 10.8 GHz (135 to 174 GHz for the millimeter-wave version). Essentially, this mode is the $TM^{\square}_{11}$ mode that would propagate in the roughly rectangular waveguide formed by the two ridge inner surfaces and the two sidewalls in Figure 8. The wall currents should be largely longitudinal, hence the longitudinal "side grooves" (see Figure 8) and the dimension Y have no influence. The E fields would be both longitudinal near the system axis and (for frequencies above the lower-cutoff frequency) radial with respect to the axis. Thus, the ladder rungs would for the most part (and especially at the low end of the passband) act like thin wires perpendicular to the E-field lines (much as in certain extended-interaction klystrons).

The guide wavelength for this "forward-wave" mode varies from infinite (no reversals of the purely axial E field) at the lower cutoff to 2P (one reversal of the axial E field per ladder period) at the upper cutoff. If Figure 14 were extended somewhat beyond its right-hand edge, one could predict a possible beam/wave interaction around 10.7 GHz and for $\theta = 245^{\circ}$, approximately. In fact, the conditions for backward-wave oscillation are manifest. Working against the possibility of these oscillations starting, however, are the very high frequency (170 GHz for the millimeter-wave version) and low group velocity and consequently high circuit attenuation. Importantly, the applicable value of β, reflecting both the high frequency and the space-harmonic aspect ($\pi < \theta < 2\pi$), would be so high that only those few electrons virtually grazing the rungs could contribute to the indicated interaction.

4.4 LOWER CUTOFF FREQUENCY

When $\beta p = \theta = 0$, the guide wavelength is infinite, and both ladder modes are purely TE modes with only transverse rf wall currents under this "cutoff" condition. Thus, it would not matter then if the arrays of ladder rungs were replaced by continuous conducting surfaces. With this reasoning, both ladder modes are seen to have the same lower cutoff frequency, which would be zero if the four "side grooves" (Figure 8) were altogether open. In Figure 14, the ω-β curves for the two ladder modes are drawn with a solid line for this case.

However, there are obvious practical reasons why the depth of the side grooves (dimension Y in Figure 8) must be limited to a reasonable value. The lower cutoff frequency will accordingly rise (dotted curves at the lower left in Figure 14) as Y is reduced, since the determinants are the same as for simple ridged rectangular waveguides. For the most part, the portion of the ω-β curve accounting for beam/wave interaction (2.6 GHz, $\theta = 60^{\circ}$) is indifferent to the actual lower-cutoff frequency and the shape of the curve below about 2 GHz. Thus, a lower limit on Y can be stated in terms of not altering the curve significantly above 2 GHz. In Figure 12, four metal inserts may be noted, forming side grooves and establishing Y = 27 mm, approximately. The lower cutoff frequency is then about half the operating frequency, with negligible effect on any of the three ω-β curves (Figure 14) above 2.3 GHz. (Needless to say, the dimensional tolerance on Y can be very generous.)

4.5 EQUIVALENT-CIRCUIT MODELING

The slow-wave periodic structures under discussion are readily modeled by means of an equivalent circuit, with very good precedent. [1,6,23] This powerful technique will be reviewed and used to predict "matching impedance" and to challenge a proposal for differential attenuation modification for the two ladder modes.

To begin, the five-element circuit of Figure 15, representing one period of interaction structure, can account for the dispersion and

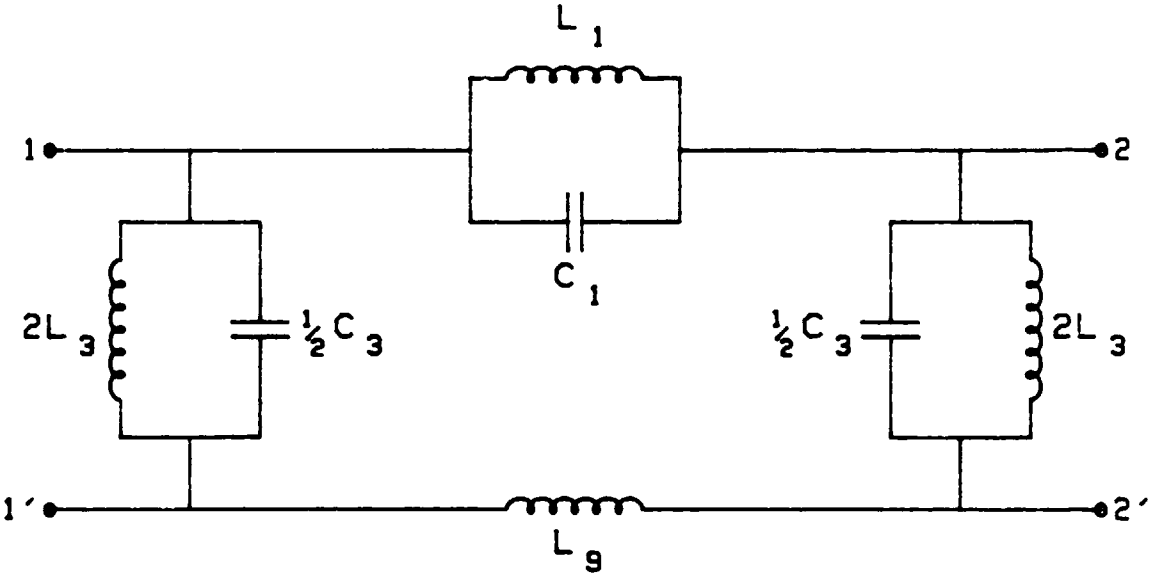

	SYMMETRIC LADDER MODE	ANTISYMMETRIC LADDER MODE
L_1	7.187 E-9	3.593 E-9
C_1	3.780 E-13	1.890 E-13
L_3	7.248 E-8	7.248 E-8
C_3	1.783 E-13	1.783 E-13
L_9	1.088 E-9	1.088 E-9

IN RATIONALIZED MKS UNITS

Figure 15. One cell of equivalent circuit for structure of Figure 12 and two ladder modes of Figure 14 - - with lower cutoff at 1.5 GHz. (Impedance relations have been observed in the relative but not absolute sense.)

impedance levels of the structure of Figure 1 if the following are observed:

- $(L_1C_1)^{-1/2}/2\pi$ should equal the resonance frequency of the ends-shorted two-conductor transmission line that exists between adjacent ladder rungs or tapes.

- $(L_1/C_1)^{1/2}$ should equal the surge impedance (characteristic impedance) of this same transmission line.

- $(L_3/C_3)^{1/2-1/2}/2\pi$ should equal the cutoff frequency of the ridged waveguide one obtains with the ladder replaced by a continuous conducting sheet -- assuming the side grooves have been closed off to provide a non-zero "lower-cutoff" frequency.

- $(L_3/C_3)^{1/2}$ should equal the surge impedance of this ridged waveguide, evaluated well above cutoff, and effective between the center of the ladder and the center of the ridge, with C_3 including the effect of any dielectric placed in that position.

- L_9 should be a small inductor which (in combination with the effective capacitance presented by the L_3-C_3 "tank" at frequencies above its resonance) would account for the phase delay over one period of distance in the ridged waveguide if L_1 and C_1 were shorted out.

When a cold-test model corresponding to a proposed geometry is not available, the element values can be predicted with the methodology indicated above in combination with the familiar engineering methods used to estimate transmission-line resonances and surge impedances and ridged-waveguide cutoff frequencies, given the geometric details.[23] However, when a model has been built, measured ω-β data can be processed with long-established computer routines to yield the element values and regenerate ω-β curves for checking purposes. In this case, the circuit of Figure 15 would be one of the Curnow equivalent circuits.[24]

As for the geometry of Figure 8, it is sufficient to separate the structure into two halves along the "rung-pair interface" plane and consider each half in isolation while applying the methods described. After modeling the symmetric ladder mode, a conducting surface can be introduced in the aforementioned plane to permit modeling the antisymmetric mode. In the case of Figure 14, element values (per Figure 15) were found that were consistent with each of the two ω-β curves. In particular, L_3, C_3 and L_9 could remain the same for both modes, while the change from the symmetric to the antisymmetric mode was effected rather well by halving C_1 and L_1, all as would be expected from physical reasoning.

Among the computer-output listings vs frequency is the "image impedance" -- the impedance "looking into" a semi-infinite chain of identical cells from the port 1 - 1'. In developing a waveguide input or output coupler for the interaction structure, the "image impedance" is an indicator of the load presented to the waveguide. With regard to the eventual narrow-band TWT, it is therefore encouraging that, for the symmetric ladder mode, the "image impedance" was found to vary very little with frequency over an appreciable range around the operating frequency, f_0.

With the two modes represented by two only slightly different versions of the circuit of Figure 15, issues may be raised and quantitative predictions made. For example, it had been naively suggested that if dissipative materials were placed in the "side grooves" (Figure 8), the resulting attenuation at f_0 might be much greater for the antisymmetric mode than for the symmetric. (The reasoning here correctly noted that at f_0 the symmetric mode has a low phase velocity, suggesting energy propagating close to the rungs, while the antisymmetric mode has a high phase velocity, suggesting more energy propagating in the side grooves.)

To test this differential-attenuation hypothesis, computer routines associated with Curnow equivalent circuits were used to calculate circuit attenuation per period when a resistance was introduced in parallel with L_1 and C_1 and/or L_3 and C_3. This resistance was quantified by specifying a finite Q to be associated with each inductance. Specifically, relatively low values were assigned to Q_3, to represent the dissipative material

proposed for the ridged waveguide, while the Q_1 values considered reflected no added loss for the ladder rungs. If the unit cell were visualized as having an overall effective Q, this would indeed be influenced by Q_3 much more in the antisymmetric mode than in the symmetric mode at f_0 (as implied by the different phase velocities).

The results of the final computations clearly refuted the naive hypothesis. In every case, the attenuation (dB/period) at f_0 for the symmetric mode ended up as great as, or even greater than, for the antisymmetric mode. In physical terms, what was quantitatively demonstrated was the importance of group velocity to circuit attenuation. At f_0, the group velocity for the symmetric mode is so much lower that it offsets or more than offsets the reduction in infuence of the ridged-waveguide loss. In fact, the necessity of minimizing ridged-waveguide losses in the eventual TWT is now apparent, lest the low operating group velocity (0.05c) magnify their contribution to the burden of total circuit attenuation.

5.0 RF CIRCUIT ATTENUATION

Reliable data on the attenuation per unit length of the slow-wave structure, at and around f_0 and at the applicable temperatures, are a prerequisite to gain/bandwidth predictions for the eventual millimeter-wave TWT. Ideally, a length of actual-size interaction structure (Figure 8) several dozen periods long would be made up and heated, as necessary, during attenuation measurements around 42 GHz. (The Steele method would permit these measurements to be made without requiring good input and output couplers.) This enterprise, however, is reserved for a future date. Substitution of a scaled-up circuit model can be considered, provided it is relatively long and means are at hand to account for the frequency dependence of rf skin resistivity for the metals and brazing materials involved. Accounting, in addition, for a non-negligible dielectric loss per period (which is independent of frequency if the loss tangent is) would not be an easy matter in a scale model, even if diamond were not the dielectric in question. The millimeter-wave effects of surface roughness are also hard to transfer to a scale model.

For the present contract, attenuation values are of necessity theoretical, and hopefully supported by advanced scientific insights. The most convenient and powerful approach here has been through use of the relation[25]

$$\text{attenuation in dB/cm} = \frac{8.686\ \pi\ f}{Q\ \ v_g}$$

where the frequency, f, is in Hz and the group velocity, v_g, is in cm/sec. The Q here would be a composite value for one unit cell of interaction structure, taking account of each component element where energy might be stored and power dissipated. The entire circuit-attenuation problem is now merely one of establishing Q, and for engineers, Q has considerable reality, given the frequency and materials selected. Over the TWT bandwidth, moreover, the possible variation of Q would be very small relative to the variation of the term f/v_g.

Two of the unit-cell component elements referred to above are the capacitances influenced by the diamond dielectric. Even assuming no surface contamination whatever, no basis as yet exists for quantitative loss estimates here, hence one can only assume for now that such losses will contribute much less to the overall Q than might others. Similarly, for now, the wall losses of the ridged waveguide will be assumed to contribute much less than does the one remaining element -- the relatively delicate copper tape pair constituting an individual ladder rung. In sum, the Q of a rung is to be evaluated and then assumed to approximately equal the overall Q of a unit cell or perhaps exceed it by a factor of, say, 2.

For this evaluation, the two tapes forming one rung will be assumed to be in contact over their entire length, as if the beam tunnel were squeezed out of existence. (Little error should result from this simplification since rf rung currents are weak around the center where the actual tapes are not in contact.) The rung cross-section would then be 0.13 x 0.15 mm (5 x 6 mils) and the Q would be $\pi Z_0/4R$ where Z_0 is the surge impedance of the two-conductor transmission line (separation 0.18 mm or 7 mils) existing between successive rungs (see right side of Figure 8). Considering only distributed resistance along a rung, R is half the skin-effect resistance along one edge of one rung (from anchor point to anchor point).

The estimate Z_0 = 230 ohms may be arrived at using traditional methods.[26] Concerning resistance, the surface resistivity of copper at 42 GHz is 0.054 ohms per square; however, this applies only to "room temperature" and neglects any difference between Amzirc and copper and the contributions of "anomalous skin effect" and possible surface roughness -- both significant above 30 GHz. With this surface resistivity, the estimate R = 0.27 ohm may be arrived at, with allowance made for the fact that the edge of a rung is effectively wider than 0.13 mm (5 mils) because some of the rf current flows on adjacent tape surfaces.

With Z_0 and R as above, one has Q = 670, which is clearly optimistic for the several reasons given. Most of the predictions of the next chapter were based on Q = 500, which is lower, but very likely still optimistic. A few of the calculations were repeated for Q = 250, permitting the effect of

this difference on gain and efficiency to be noted. At 42 GHz and v_g = 0.053 c, circuit attenuation would be 0.047 dB per period (1.44 dB/cm) for Q = 500, or double that attenuation for Q = 250.

6.0 INTERACTION MODELING

6.1 GENERAL

The "Tunneladder" slow-wave structure (Figures 8 and 12) was devised to provide a high interaction impedance and hence a potentially high rate of gain per unit length in interaction with a suitable electron beam. Computer simulation of a TWT embodying this beam and circuit was undertaken to confirm the structure's promise. The necessary software was provided by the codes described in the current Varian Helix-TWT Computer Program Users' Manual. The foundation for dealing with a Tunneladder TWT much as a helix TWT was discussed previously.

To start with, the not-quite-circular tunnel region of the interaction structure was assumed to be exactly circular, as if there were a helix with I.D. and O.D. of 9.75 and 11.79 mm, respectively. (The modeling was based on S-band dimensions and frequencies, though Q values are to reflect millimeter-wave conditions.) A beam diameter of 6.50 mm (filling factor 2/3) was assumed, along with a helix-shielding "barrel" diameter of 19.91 mm (suggested by the inner faces of the ridges). Importantly, the small azimuthal variation of rf fields within the beam cross-section was considered as negligible.

In addition to the diameters given above, the effectively tubular circuit was represented for interaction modeling purposes by the measured ω-β curve (curve E in Figure 13 and lowermost curve in Figure 14) and on-axis sapphire-rod perturbation data (E at bottom of Figure 13). By processing the ω-β data, the curves of phase velocity ($= \omega/\beta$) and group velocity ($= \partial\omega/\partial\beta$) vs frequency of Figure 16 were produced. Figure 16 also shows how circuit attenuation might vary with frequency. (Spline-function interpolation was used to provide continuous curves between original-data points spaced relatively widely in frequency; as noted in Figure 16, the 1% of eventual hot bandwidth is small compared with this frequency separation.)

This done, the original sapphire-rod frequency-perturbation data could be processed to yield the on-axis Pierce impedance. The methods used here

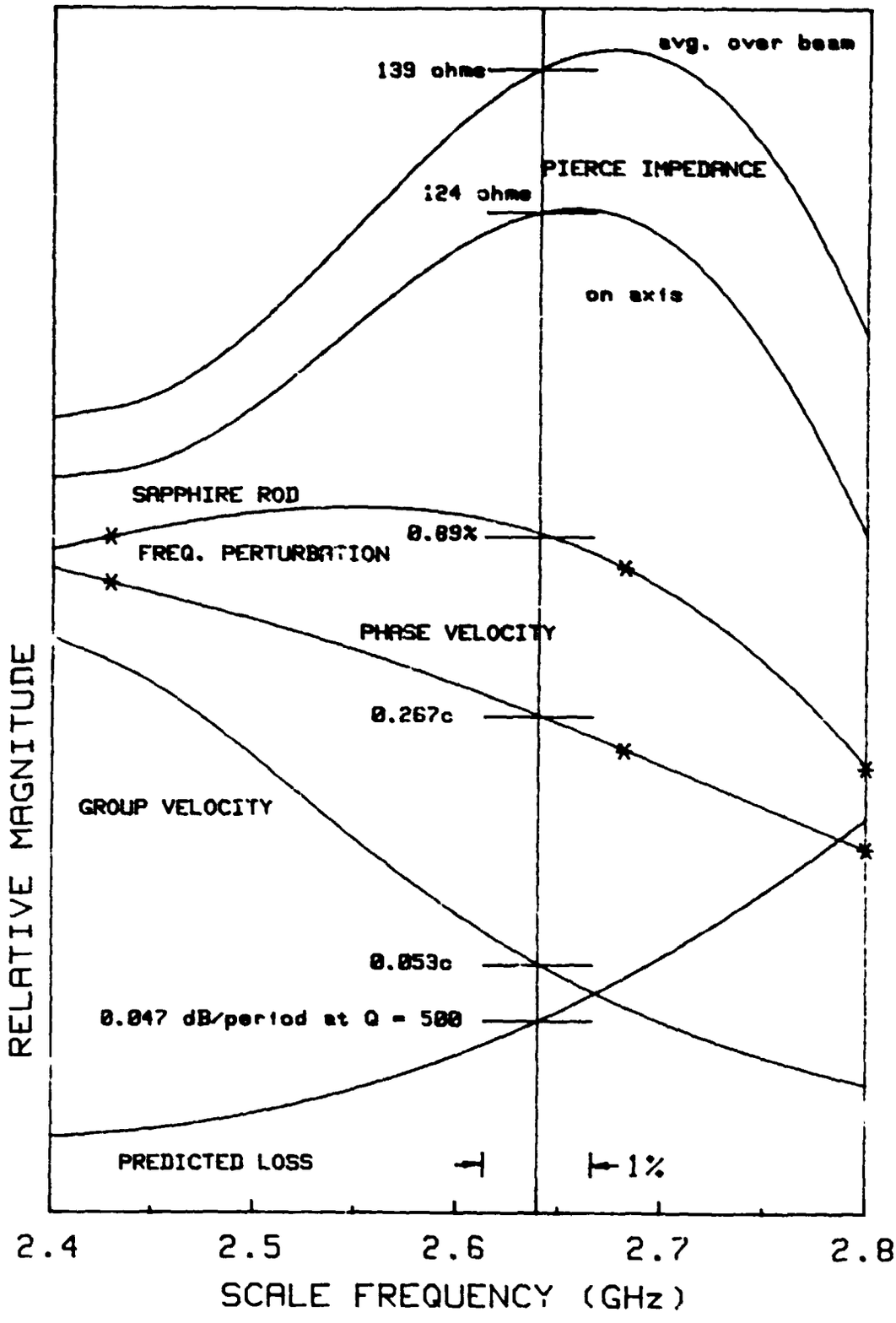

Figure 16. Measured and derived TunneLadder interaction parameters.

were standard and include the "Lagerstrom correction" for error due to the non-zero rod diameter. Given the tubular circuit representation and the assumed beam filling factor, standard methods were also available for establishing a Pierce impedance averaged over the beam cross-section. These impedances are frequency dependent (see Figure 16) and appear to peak close to the proposed operating frequency (2.64 GHz for the scaled model). This felicitous result suggests that the tunnel geometry has been optimized so that at $\theta = 60^{\circ}$ an ideal balance has been struck between the increases with β of the impedance close to the rungs and of the rate of decay of axial E fields from the rung vicinity toward the system axis. As far as is known, this occurrence is altogether fortuitous. The Pierce impedances achieved around 2.64 GHz -- well over 100 ohms -- would be considered quite respectable by helix-TWT standards.

6.2 SMALL-SIGNAL SIMULATION

To predict the gain and bandwidth of the hypothetical TunneLadder TWT, a postulated confined-flow beam microperveance of 0.06 seemed reasonable. Higher values might be considered, but the small-signal gain would only increase roughly as the 1/3 power of the perveance, while the beam-interception power would increase at least linearly. The interception power might increase even faster since the percentage interception would worsen without an increase in the focusing field. True, the increased perveance could lead to some tube-length reduction (roughly as 1/3 power of perveance) so that a somewhat stronger focusing field might be obtained with the same weight of magnet material.

The hypothetical TWT was also postulated as having two sections with 50 periods per section and a zero-length "sever". Accordingly, the small-signal gain-vs-frequency curves one may predict through the simulation procedures are as shown in Figure 17, where the effects of changing the beam voltage or the assumed effective circuit-cell Q are also indicated.

Examining these curves, the center frequency of the "hot" passband is seen to tune with beam voltage. This voltage-tuned-amplifier capability could be useful, since different communication channels could be selected by

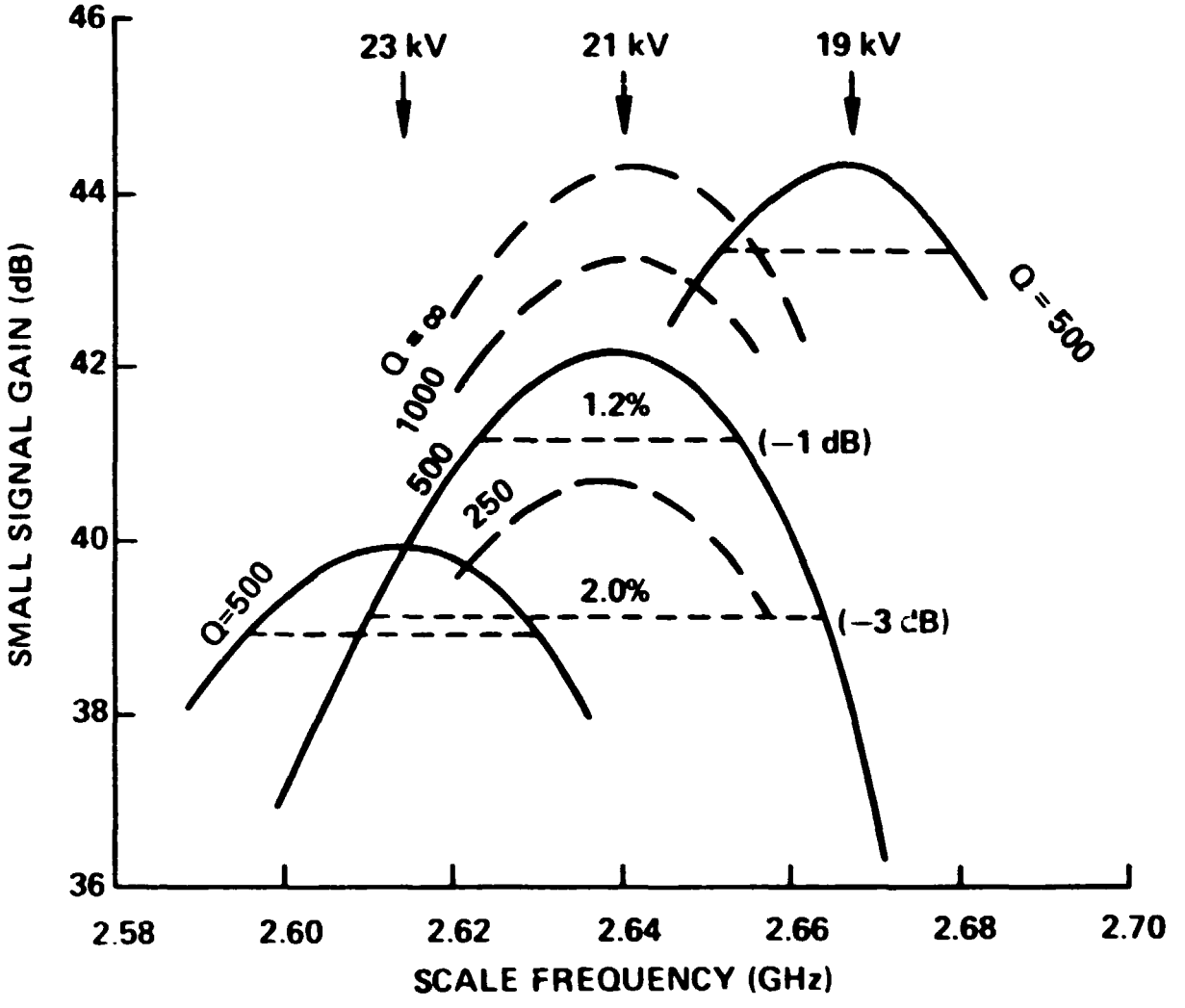

Figure 17. Beam-voltage and Q dependencies of small-signal gain curve of hypothetical two-section TunneLadder TWT.

changing the voltage and not the tube design. Each such channel, of course, would retain the narrow instantaneous bandwidth which, at 21 kV and Q = 500, is 1.2% or 2.0%, respectively, for the "1-dB down" or "3-dB down" definitions. (It may be noted, under constant Q, that as the voltage is increased there is also a slight increase in instantaneous bandwidth and a small decrease in peak gain.) The data of Figure 17 also suggest the sensitivity of the channel center frequency to beam-voltage mis-regulation -- when this frequency is elected to be fixed.

In view of the uncertainty regarding the projected effective circuit-cell Q, the actual effect of this Q on the small-signal gain curve was included in Figure 17. At 21 kV, the peak gain may be noted to drop perhaps 4 dB as Q decreases from infinity (lossless circuit) to 250 (0.094 dB/period). As is characteristic of many TWTs, a given circuit attenuation has less net impact when the gain rate (represented here by BCN = 0.5 dB/period) is high.

To complete the small-signal modeling, the sensitivity to the assumed beam filling factor was examined and found minimal: the filling-factor increase from 0.667 to 0.700, for example, added only 0.3 dB to the total small-signal gain of the simulated TWT. (The effect on efficiency and large-signal gain -- see below -- was similarly trivial.)

6.3 LARGE-SIGNAL SIMULATION

Prediction of the ultimate helix-TWT output power and conversion efficiency is based on large-signal analytic routines that are "one-dimensional" (no variation across any beam cross-section) and "distance stepping". The computer cost per run is substantial, relative to small-signal runs, hence only one signal frequency (2.64 GHz) and one beam voltage (21 kV) were considered, along with the same circuit and beam parameters as before.

The computer outputs "flight line" diagrams as well as a tabulation gain rate and rf power level as a function of interaction distance. A sufficiently high rf input power level is postulated such that "saturation"

will be reached within a short enough distance along the structure. Accordingly, a conversion efficiency of 21% was projected at saturation for an assumed circuit-cell $Q_c \approx 500$. (The corresponding "saturated" gain is 8 dB less than the small-signal gain for this hypothetical TWT.) This efficiency suggests a "saturated" power output of 800 W (and naturally, some increase in bandwidth under "large-signal" operation). If only 200 or 250 W of output were required, the tube could be considered a "linear" amplifier, with a "depressed collector" used to recover the overall efficiency. Given the nature of the spent beam in this case, the depressed collector here would be effective and economical to implement.

If a better estimate of the effective circuit-cell Q were 250 rather than 500, the "saturated" efficiency and output power would drop to 18.7% and 710 W, respectively. Of course, any such power levels might not be attainable if heating or rf voltage breakdown imposed a lower limit.

6.4 RF VOLTAGE STRESSES

It is possible that the rf power rating of the proposed tube will be limited by rf voltage breakdown rather than by beam saturation (previous section) or by overheating (next chapter). Centrally maximum rf voltages are developed from tape to tape and from tape to ridge, with breakdown therefore possible along the surface of a diamond support rod near the TWT output end. No data are on hand regarding the "insulation strength" of a polished (or perhaps intentionally roughened) diamond surface, even if completely uncontaminated. Moreover, the effects of shape and roughness of the Amzirc tape edges, where bonded to the dielectric, cannot as yet be accounted for. The best that can be done here is to determine the constant of proportionality between the maximum rf field intensity and the square-root of the output power, permitting the tube rating to be decided at such time as the relevant "insulation strength" becomes known.

Through study of the equivalent circuit of Figure 15, as one cell in an infinite chain, one can establish that around 2.64 GHz and $\theta = 60^{\circ}$ the tape-to-tape voltage, V_1, is rather comparable in magnitude to the tape-to-ridge voltage, V_3. However, the breakdown path lengths for V_1 and V_3 would

be in the ratio of 7 to 10, respectively. Consequently, attention will be focused on the axial tape-to-tape E fields as the more likely to exceed the safe limit as rf power increases. Of course, dividing voltage by distance only yields an average E field (the quantity to be evaluated below); in actuality the field close to a tape edge would significantly exceed the average.

An axial-field/power-flow relation is conveniently expressed by the Pierce impedance, $E^2/2\beta^2P$ which, at the pertinent value of β, is 124 ohms on-axis, but 1.33 times larger off-axis at the mean radius of the supposed tape helix. (All voltages here are "peak" as opposed to "rms".) The field that might then be calculated would be correct for very fine tapes; the actual average field between heavier tapes would be close to twice greater when they are as wide as they are (6/13 of the period). In sum, the (peak) tape-to-tape voltage would be around 20 times the square root of the output power in watts (e.g., 280 volts at 200 W, etc.). In the 42 GHz design, therefore, the average field between tapes, in (peak) volts/mil, would be around 2.9 times the square root of the output power in watts, or 40 volts/mil at 200 W, etc. To reiterate a point made in the first paragraph of this section, it is not at present known how close the stress of 40 volts/mil might be to the surface insulation strength of the proposed dielectric material at 42 GHz; the requisite specialized investigation is recommended.

7.0 THERMAL ANALYSIS

7.1 PROBLEM ASSESSMENT

In the proposed TWT, interaction-structure temperatures will rise as a result of both beam-interception and rf-dissipation heating and it is necessary to establish that temperatures will not exceed the allowable. This might be 400°C in a "space" tube, or something higher in an "earth" tube. If excessive temperatures are predicted in the design stage (or observed in a "hot" test) the following measures are among those that can be considered: mechanical redesign to reduce heat-evacuation resistance; electron-optical redesign to decrease beam interception; power-output derating to decrease dissipation power.

In the present prediction phase of thermal-effects assessment, brash assumptions become necessary -- not so much regarding evacuation paths and resistances as concerning the amount of heat that might be inputted at a given point The total interception power under full rf drive might be estimated at 5% of the beam power. (More implies that the tube is unlikely to amplify well; less implies that the electron-optical system is too "critically adjusted" and susceptible to upset.) However, the fraction of this likely to be intercepted in any one period is almost undefinable, given the small tunnel diameter and the paucity of experience with the corresponding electron-optical systems. Less uncertainty exists with regard to the rf power dissipated in the final circuit period insofar as an effective Q at the actual local temperature can be estimated.

Current practice is to assume the last period is the worst "hit" by beam interception as it is by rf dissipation. In this case, heat could flow away not only transversely, but axially, toward the cooler gun end of the circuit. It is planned to ignore this effect here and accept that the predicted temperature rises would then be pessimistically high in this regard. The same would apply to the decision to neglect radiation-cooling effects.

Within these limitations, the best that can be done for now is to examine some relationships between temperature rises and postulated heat inputs. Unfortunately, the inclusion of diamond in one of the two transverse evacuation paths makes the problem non-linear. Not only are temperature and power disproportional, but superposition cannot be used to account for the two possible inputs (which are somewhat correlated but only to a limited extent).

The geometric symmetries of the structure cross section (Figure 8) permit division into four quadrants for which symmetry might prevail thermally as well as mechanically. In this case, Neumann boundary planes would lie along the mid-plane through the diamond rods and along the plane designated "rung-pair interface". The distinctions between "watts per period" and "watts per period per quadrant" can be made easily enough with regard to either the beam interception or rf-dissipation heating.

7.2 BEAM-INTERCEPTION POWER ESTIMATES

Several temperature-rise predictions were based on the assumption of 10 W per period per quadrant as a possible worst-case beam-interception power input. This would apply if the total interception (under full rf drive) were 5% of the beam power (which ≈ 1 kW per quadrant) and if all of this interception essentially occurred uniformly over the last five periods. Hopefully, in practice, the total interception (if not less than 5% of the beam power) might effectively be spread over more than five periods, so that the interception per any one period might be less than the indicated 1% of the beam power. If not, it would be safest to ensure that the structure could withstand this worst-case level.

Several assumptions can be made regarding the transverse-plane distribution of this heat input. In the simplest case, the power might be assumed to be uniformly deposited over the 0.25 mm of tape where it is supported by diamond. However, it is more likely that there will be some concentration on the centerline (assuming ideal beam alignment) and also some deposition of interception power on the tape outside the diamond-supported segment. To quantify this distribution pattern, more

would have to be known about the beam-edge current-density profile (under drive) than is possible at present.

7.3 RF-DISSIPATION POWER ESTIMATES

At the "operating point" the rf power dissipated per period per quadrant can be expressed as 1.4/Q times the total rf power level. If the Q value here were to reflect all sources of loss (dielectric, sidewalls, etc. as well as tapes), the computation would yield the total power dissipated. However, if the Q is merely that of the ladder rung, one obtains only the dissipation along a rung. For now, this is the plan being followed, implying that rf power dissipated anywhere but along a rung is being ignored with regard to possible temperature rises.

The Q of a copper rung was previously estimated (Chapter 5) at about 670, at room temperature, and neglecting the effects of roughness and "anomalous skin effect". With a temperature coefficient of resistivity of about 0.004 per ^{o}C, copper's dc resistivity would double if -- as the final result of initial rf heating, reduced Q, increased dissipation, further heating, etc. -- there were a temperature rise of about 250^{o}C. The corresponding drop in rung Q would be about 30%. Of course, temperature (and hence resistivity) would vary along the length of the rung, though the coolest portion would be near the side wall where rf current is most significant. It therefore seems reasonable to attempt temperature-rise projections on the basis of Q = 500, but to consider Q = 250 as well to avoid possible overoptimism. The final-rung dissipation per quadrant would then be about 1/360 (for Q = 500) or 1/180 (for Q = 250) of the TWT output power, which is nominally 200 W, but might be 800 W for "saturated" operation.

In view of the above, rf rung dissipations ranging from 0.5 to 4.5 W per quadrant might be considered for temperature-rise projections (with interception heating occurring at the same time). The rf energy would, of course, be assumed to be deposited along the tape as an increasing function of distance, x, from the center. Specifically, the function $\sin^2(\pi x/2\ell)$ should be a good approximation, where ℓ is the developed tape length from

center to sidewall. In this case, about 82% of the power in question would be generated in the outermost 0.6 mm (per Figure 8) of the rung span -- essentially the portion where the tape is flat and perpendicular tc the side wall.

7.4 PRELIMINARY TEMPERATURE ESTIMATES

Figure 18 suggests how the features of the interaction structure of Figure 8 might be adapted to enhance the thermal capability of the eventual TWT design. Two axial coolant ducts (or equivalent heat-sink means) are proposed for the "sidewalls" such that a minimum thermal resistance is obtained between the "coolant" and the rung anchor points. Two additional axial coolant ducts are proposed for the base of each ridge, similarly minimizing the thermal resistance between the coolant and the diamond rods. In pursuance of this objective, a tall ridge would be undesirable, hence the "side grooves" of Figure 8 might be modified in profile (per Figure 18) to permit both a short ridge and a low lower-cutoff frequency (Figure 14). Current practice is to assume a coolant temperature of 100°C ("tube body temperature") when predicting temperature rises deeper within the tube.

A preliminary assessment of the temperature-rise situation was attempted by assuming complete separation of the two heat inputs and the two evacuation paths. This is tantamount to cutting the rung tape so that beam-interception heat may exit only via the diamond rods, and rf-dissipation heat only via the sidewalls. Some valuable guidance was obtained in this way, and later analysis (next section) indicated that the results obtained were reasonably valid in all but some extreme cases.

Proceeding accordingly, a 0.063 x 0.15 mm tape was assumed severed about 0.6 mm from the sidewall anchor point and the rf rung dissipation power per quadrant was inputted uniformly along this tape segment. Assuming a temperature-invariant thermal conductivity of 3.88 watts per cm per °C, a "linear solution" of 80°C per watt per period per quadrant would then be obtained for the hot-point temperature. On this basis, a rung dissipation

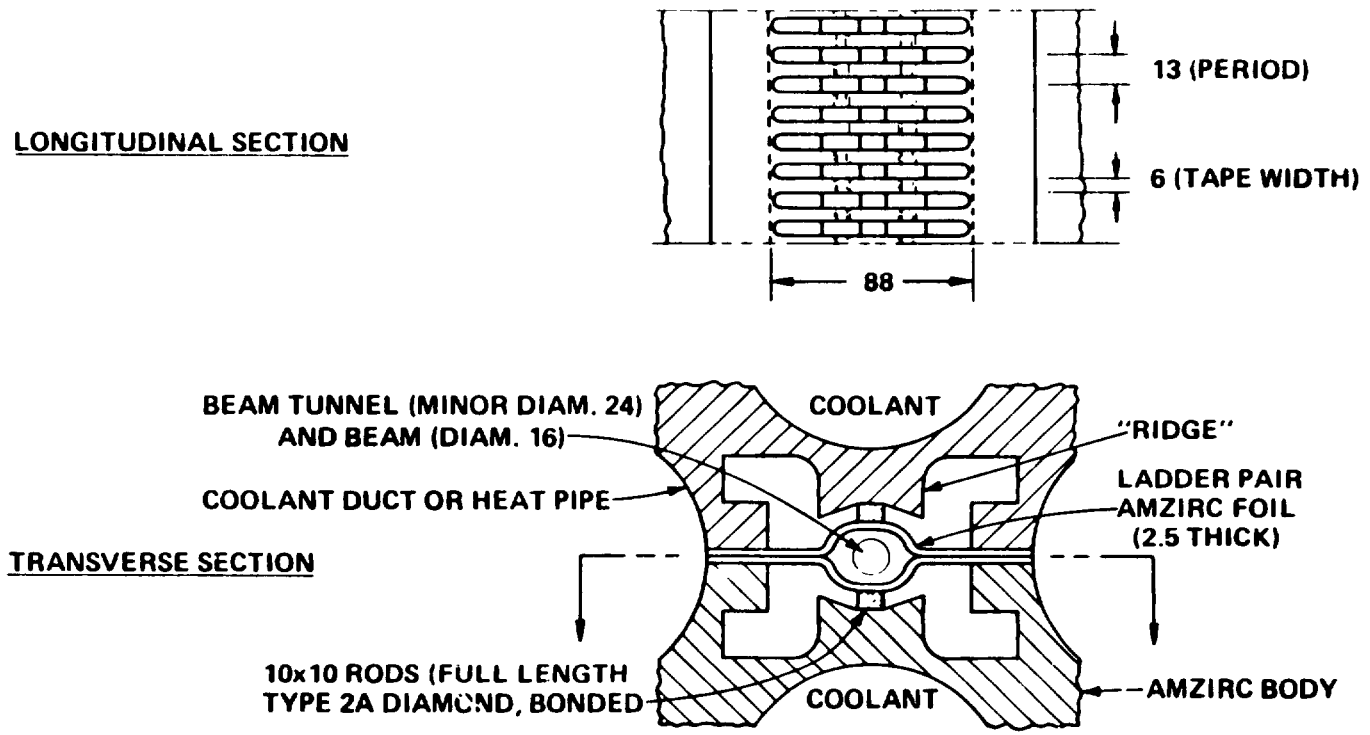

Figure 18. Practical "TunneLadder" TWT design developed from Figure 8. (Dimensions stated in mils for 42 GHz operation.)

up to 5 W per quadrant might be tolerated without exceeding 400°C. As discussed in Section 7.3, the actual rung dissipation power is anticipated to be between 0.5 and 4.5 W per quadrant.

As for beam-interception power, the amount impinging on one tape (two quadrants) is assumed to start flowing outward through 0.25 mm of diamond where the cross section is 0.25 mm x 0.33 mm, which is one period. (This requires simplifying assumptions about the spread of heat from the tape to the diamond and the neglect of any axially directed heat flow.) The heat is then assumed to spread immediately across the copper ridge, with a cross section of 1.1 x 0.33 mm, and travel 0.5 mm to the base of the ridge. On this basis, the "linear" temperature drop from top to base of ridge might be about 7°C per watt per period per quadrant, or 70°C for the "worst-case" interception level stated in Section 7.2

For the non-linear portion of this problem, one may express the temperature difference across the diamond in °C as 15.6/M per watt per period per quadrant, where M is the thermal conductivity of diamond relative to copper, suitably averaged over the temperatures that might prevail within the dielectric. From Figure 11 it can be seen that M must lie between 5 (100°C everywhere) and 3 (400°C everywhere). Thus, for the "worst-case" interception level stated in Section 7.2, the temperature difference across the diamond rod might range from about 30 to 50°C, which in any case is less than the drop from the top to the base of the ridge.

7.5 COMPUTER THERMAL MODELING

Figure 19 was prepared to represent to scale one quadrant of one period of the interaction structure for thermal-modeling purposes. As may be noted, the rung or tape has been pulled out straight (which has little effect thermally when radiation is ignored) and division into cells has been instituted. Each cell has one or more numbered "nodes". Nodes 29 - 42 and 45 - 56 identify the tape, and 14 - 15 and 19 - 28 the diamond. All nodes below 14 and 15 belong to the ridge and all nodes to the right of 42 belong to the sidewall mass of copper per Figure 18. The dimension of all cells normal to the diagram is the period, except for the cells of the tape for

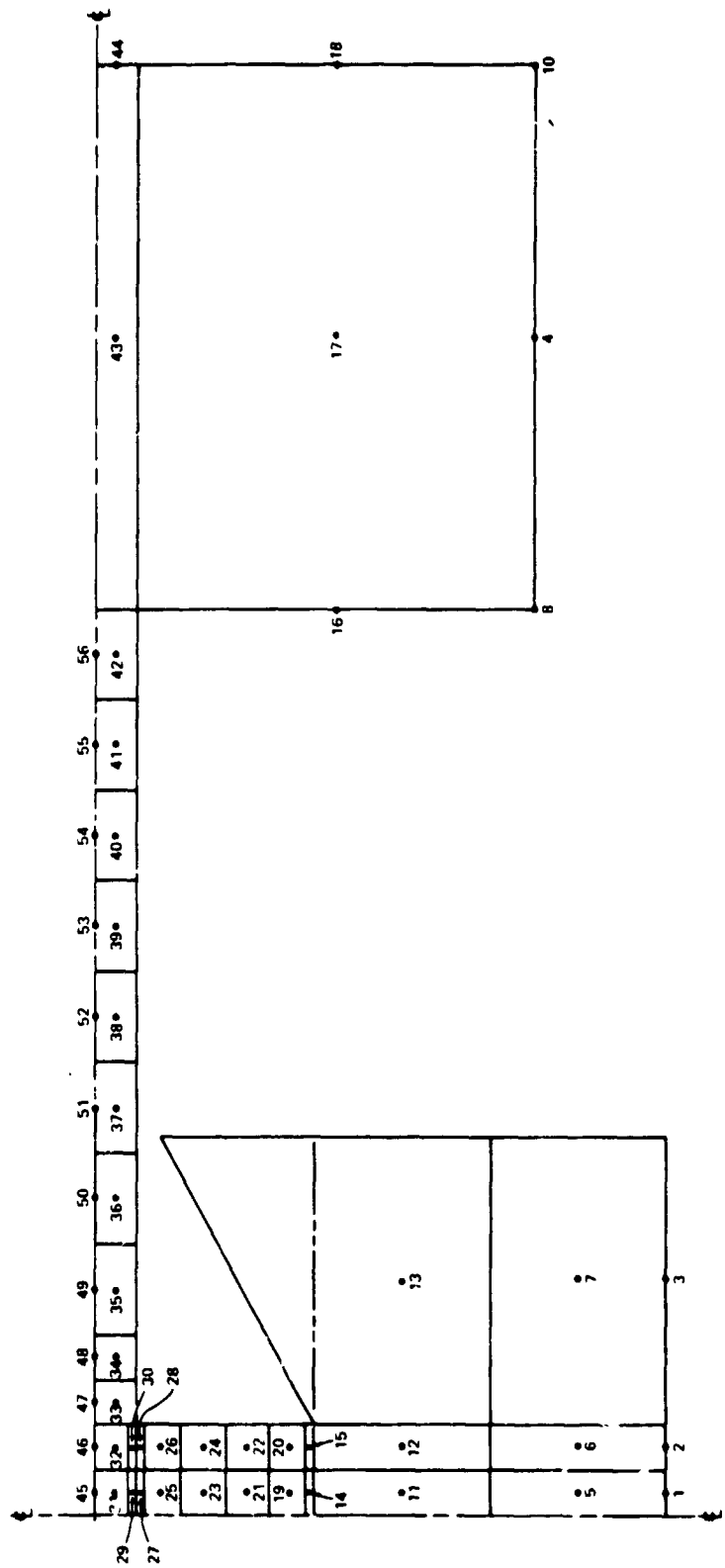

Figure 19. One quadrant of one period of interaction structure with cells and nodes for computer thermal modeling.

which the amount is 46% of the period. The temperatures of nodes 1 - 3, 10, 18 and 44 are assumed fixed at 100°C. Figure 11 provided the thermal-conductivity values with the temperature variation neglected only in the case of copper.

This representation was used in conjunction with program VULCAN to relate node temperatures to heat input via the methods of rheology. Smaller cells provide greater accuracy, but more effort is required to input the numerous resistances connecting each node with its neighbors. The small cells 14, 15 and 27 - 30 are intended to increase accuracy where there is a change in material or a change in the dimension normal to the diagram. The omission of a small cell between 42 and 43 may therefore decrease accuracy as does the large cell size at 7 and 13. (This latter became evident after interpretation of the final results; given the time available, desirable refinements could be identified but not implemented.)

The total beam-interception power per period per quadrant, P_{bi}, was inputted to nodes 45 - 47 in the amounts of 50%, 37.5% and 12.5%, respectively, to suggest the way interception power might be distributed in the transverse plane. The total rf dissipation power per rung per quadrant, P_{rfd}, was inputted to nodes 48 through 56 in amounts of 1.5% through 19.8%, respectively, to suggest the sine-squared distribution discussed in Section 7.3. (The node series 48 - 56 is essentially redundant to the series 34 - 42 in view of the negligible thermal resistance between corresponding nodes.)

The results of a VULCAN run include a tabulation of the steady-state temperatures reached at the various nodes. Also outputted are P_{DR}, the thermal power exitting via the diamond and ridge, and P_{SW}, that exitting toward the sidewall. To the extent that $P_{DR} \longrightarrow P_{bi}$ and $P_{SW} \longrightarrow P_{rfd}$, the separation-of-effects concept of Section 7.4 is validated. This seems to be the case (see below) except when $P_{bi} \ll P_{rfd}$ or vice versa.

Some typical results are summarized below, covering two hypothetical levels of P_{bi} and four of P_{rfd}. Within the limitations of the methods used,

these data can suggest how the proposed structure might respond to its thermal challenges and what the limitations might be.

Run	P_{bi}	P_{rfd}	P_{DR}	P_{SW}	temperature maximum (^{o}C)	at Node
	(watts per period per quadrant)					
1	10	0	8.9	1.1	379	45
2	10	1.5	9.5	2.0	394	45
3	10	3.0	10.1	2.9	409	45
4	10	4.5	10.7	3.8	459	51
5	0	1.5	0.6	0.9	174	53
6	0	3.0	1.2	1.8	248	53
7	0	4.5	1.8	2.7	323	53

Implicit in the above data is the apparent thermal resistance of the ridge -- $17^{o}C/W$ on a per-period per-quadrant basis. This seems higher than is reasonable and is very likely an artifact of the excessive cell size adopted at 7 and 13. (If so, the predicted temperature rises would be pessimistic.) The apparent, effective thermal resistance across the diamond (per period per quadrant) is in the vicinity of $3^{o}C/W$ (= 5 times "better" than copper) when the heat flux is low (Runs 5 to 7) and in the vicinity of 4.4 to 4.9 $^{o}C/W$ (3.2 to 3.6 times better than copper) when the heat flux is high (Runs 1 to 4).

8.0 OTHER FEATURES OF EVENTUAL TWT

8.1 LADDER FABRICATION

It is intended at this time to suggest only a few tentative fabrication options for the shaped ladder halves of a millimeter-wave TunneLadder interaction structure. If the ladder were to be flat, the approach of winding Amzirc ribbon on a suitable frame would clearly be a strong candidate. This would lead to the least surface roughness and the cross-section shape might be selected so as to maximize the tape-to-tape rf breakdown voltage. Computerized winding machines now standard for helix TWTs would ensure low cost and uniformity of the period. The need to shape the ladder to form a half tunnel might not deter one from choosing the winding approach if the rungs could remain parallel and uniformly spaced during the requisite deformation. This might be implemented by soldering the flat ladder to a supporting sheet of foil before shaping, and then dissolving away the foil at some later time.

Laser machining might provide a very different approach since one would start with a plain Amzirc foil and shape it (to create half the tunnel) before slitting it into rungs with a computer-controlled scanning laser beam of very fine diameter. Ordinarily, copper's high thermal conductivity presents grave difficulties for laser machining, but the thinness of the foil in the present case changes that picture. Other difficulties formerly associated with copper's high infrared reflectivity have been overcome by halving the laser wavelength, producing a green-appearing cutting beam. The major drawback, however, resides with the relatively rough surface associated with laser cutting, though quantitative data have not been examined, nor has the possibility of slowing the scanning speed to obtain a smoother cut.

Photo-etching (or "chemical milling") can nowadays leave a fairly smooth finish on copper, and it is now also possible to select the angle desired between the edge of the cut and the surface of the original foil. Thus, it would be easy for the ladder rungs to have a trapezoidal cross-section (probably not possible with laser or discharge machining) with

the wider face intended to rest against the diamond support rods. It is believed that this would maximize the rung-to-rung rf breakdown voltage. As for the shaping of the ladder, the best procedure should be to apply and "expose" the "resist" while the Amzirc foil is flat, followed by shaping of the foil and then etching the slits between rungs (and dissolving the remaining resist).

Electron-discharge machining (EDM) can certainly be used to slit a foil after the requisite shaping, if one is willing to invest in the necessary "burning" tools -- an array of "burners" if all the slits are to be cut in one pass, or one burner (which would wear out much more rapidly) if the slits are to be cut successively. The eventual surface finish would require consideration along with the probable limitation to perpendicular-only cuts.

8.2 INPUT/OUTPUT COUPLERS

Transitions between rectangular waveguide and the interaction structure are clearly necessary for the input and output of an eventual TunneLadder TWT, but their design and development should be facilitated by the narrowness of the bandwidth of interest and the prediction that the "image impedance" varies little over the applicable frequency range (Section 4.5). It is clear that (for the correct mode) the slow-wave structure must be excited by transverse E fields, in each ridge-to-rung gap, that are equal -- and oppositely polarized at a given instant of time. In this regard, the TunneLadder structure resembles coupled-cavity structures that use pairs of coupling apertures,[27] and the same coupler-design principles should be applicable.[28]

In this case, the longitudinal axis of the waveguide is normal to the interaction-structure (or beam) axis with a broad wall of the waveguide providing an interface with the truncated end of the periodic structure. Moreover, the longitudinal axis of the waveguide is aligned with the ladder plane ("rung-pair interface" in Figure 8). Thus, when the interfacing broad wall is suitably and symmetrically apertured, the desired E-field amplitudes and phases will be obtained. Very likely, a single central circular aperture would suffice to provide two suitable ridge-to-rung voltages in the

TunneLadder case. (This aperture would be concentric with a smaller round hole in the opposite broad wall, through which the electron beam would enter and traverse the waveguide.)

Other features of the rectangular waveguide would be its reduced height (and the necessary taper from standard height) and the familiar adjustable "short" located just beyond the coupling region. Additional adjustable reactance-tuning elements could be introduced into the waveguide, between the coupling region and the conventional "window". In the coupling region, the greatest possible degree of symmetry about the ladder plane is desired to minimize excitation of the "fast-wave" antisymmetric mode (Section 4.3.2). In fact, one can consider introducing special screws (with axes normal to the ladder plane) into the waveguide, to be adjusted so as to counterbalance any residual asymmetry when tube operating temperature has been reached. All such "trimmers" are typically effective only over narrow bandwidths, but narrow bandwidths are fortunately sufficient here.

8.3 "SEVER"

High-gain, broad-band TWTs of any type require at least one "sever" for stability, because a perfect "hot" match at the ends cannot be guaranteed at all frequencies for which gain is possible. The sever ensures that the total attenuation of the feedback path (circuit attenuation plus "return losses" for input and output couplers, windows, and external loads) will always exceed the TWT gain. On the other hand, the proposed TunneLadder TWT may present a special case, with its narrow amplifying bandwidth (at most a few percent), low required gain (perhaps 32 dB, "small-signal"), and the likelihood in service of fixed input and output loads. If the basic circuit attenuation were 6 dB, a sever would be unnecessary if the net "hot" return loss at each end could be set and held to at least 13 dB (VSWR = 1.6). This should not be difficult to achieve, with suitable "trimming", over the narrow bandwidth indicated. The possibility of a sever-less or "booster" type TWT should therefore be considered.

However, if a sever is deemed necessary, it could be of the "external" type often used with coupled-cavity TWTs. That is, this sever consists of

two transitions from interaction structure to waveguide (similar to those at the input and output) and two waveguide terminations. With beam focusing means other than PPM, this approach could well be the simplest. Alternatively, the sever approach used in helix TWTs could be considered. In this case the dielectric support rods would receive a resistive coating near the middle of the tube. A longer tube length would result, but this sever should also be effective in absorbing energy converted into the antisymmetric-mode "fast wave".

9.0 CONCLUSIONS AND RECOMMENDATIONS

An eleven-month study program has been completed by way of preparation for future development of a low-cost alternative TWT for 42 GHz communications systems. During this program, a new interaction structure (TunneLadder) has emerged, and its electrical, mechanical and thermal evaluations (via scaled cold-test modeling and computer-supported analysis) lend validity to the basic NASA-originated design premise. This premise advised sacrificing bandwidth in a millimeter-wave space-communications TWA for the sake of a very high interaction impedance and the many resulting advantages, such as a short interaction length, a relatively small focusing magnet, and a lessened impact of circuit attenuation on gain and efficiency.

The recommendation of maximizing gain per unit length via interaction with the fundamental Bloch wave of a "forward-wave" circuit was also followed, along with the advice to select a periodic slow-wave structure based on a ladder that could be fabricated by some means other than the axial stacking of cup-like cavities (which would be numerous, diminutive and costly for a 42 GHz amplifier). However, the ladder-based interaction structure selected was not flat, but adapted to accommodate a pencil beam.

In view of all the design premises stated, commonality with helix-TWT features was perceived -- except for the high-impedance and narrow-bandwidth aspects -- and recent millimeter-wave advances in this art were reviewed. The new technology of diamond support rods was thereupon co-opted, and its benefits further enhanced by introducing spatial separation of beam-interception and rf-dissipation heating. In consequence, a power-handling capability predicted to exceed that of the helix design has been obtained, as well as support means for the slender ladder rungs required by the non-space-harmonic interaction.

In particular, performance has been predicted for a beam voltage and microperveance of 21 kV and 0.06, respectively. A potential gain rate of BCN ≈ 0.5 dB/period (16 dB/cm at 42 GHz) appears obtainable, implying a short tube and a modestly sized focusing magnet. Instantaneous bandwidths somewhat over 1% have been projected; however, the possibility of electronic

tuning of the band center frequency over several percent, via beam-voltage changes of a few kV, has also been predicted. If the tube is driven to "saturation", conversion efficiencies around 19 or 21% should be possible, depending on the circuit attenuation effective at operating temperature. Preliminary thermal analysis suggests the corresponding rf power level (800 W) might well be accommodated unless rung-to-rung rf voltage breakdown imposes a lower limit. In any case, a "linear" amplifier with 200 or 250 W of output power should be viable, with a respectable overall efficiency secured by means of a depressed collector.

The serviceability of the envisioned narrow-band millimeter-wave TWT has been supported by investigations of the TunneLadder interaction structure's sensitivity to dimensional deviations. These investigations were incidental to measuring and optimizing the dispersion and impedance characteristics. Two of the periodic structure's extraneous modes of propagation have also been investigated in case certain adverse effects, identified in advance, require correction. In contrast with topologically similar interaction structures employed by other workers, the geometry of the present TunneLadder design provides per se a large frequency separation between the (symmetric) mode chosen for interaction and the potentially troublesome (antisymmetric) mode next above it.

A number of tasks remain for future work. A high priority is assigned to the in-depth evaluation of the microwave (X-band and above) dielectric properties (loss tangent, surface breakdown strength, and their temperature dependence) of Type II A diamond that has been heated in helium to 1030°C. This heating is related to the circuit fabrication, the ladder-forming aspect of which now requires concerted attention, with the possibilities of winding, photo-etching, chemical milling, laser milling, discharge machining, and perhaps other techniques to be checked out. The technique finally adopted may well influence the circuit attenuation (through roughness effects, for example) whose evaluation will require more accuracy than is evident in the analytical estimates attempted to date.

Refinements in the computer-assisted thermal modeling so far attempted are clearly desirable to improve accuracy. However, greater precision in

relating temperature rise to heat input would serve little purpose unless a more exact quantification were available of the worst case of beam interception -- the magnitude and distribution of electron bombardment of any one rung. It is also recommended that one consider possible mechanical deformations resulting from thermal gradients.

The design of a transition between rectangular waveguide (also incorporating a suitable ceramic "window") and the TunneLadder interaction structure should be undertaken, initially with scale models, as soon as the slow-wave circuit geometry is finalized -- on the basis of reliable data on diamond's dielectric properties. (It would be of considerable value to know what level of tube performance might be possible if the use f diamond had to be abandoned in favor or beryllia.) If the inclusion of a "sever" in a TunneLadder TWT were deemed essential, decisions would be required regarding its form and implementation.

10.0 REFERENCES

1. A. Karp, "Traveling-Wave Tube Experiments at Millimeter Wavelengths with a New, Easily Built, Space-Harmonic Circuit," Proc. I.R.E., vol. 43, pp. 41 - 46, (1955).

2. A. Karp, "Millimeter-Wave Valves," pp. 73 - 128 in Fortschritte der Hochfrequenztechnik, Vol 5, M. Strutt et al., eds., Academic Press MBH, Frankfurt/Main., 1960.

3. Ibid., Fig. 30 (d), p. 116.

4. Ibid., Fig. 30 (e), p. 116.

5. Ibid., bibliography items 118 - 123, p. 127.

6. A. Karp, "Backward-wave Oscillator Experiments at 100 to 200 Kilomegacycles," Proc. I.R.E., vol. 45, pp. 496 - 503 (1957).

7. L.D. Cohen, "Backward-Wave Oscillators for the 50- to 300-GHz Frequency Range," IEEE Trans. Electron devices, vol. ED-15, pp. 403 - 404, June 1968.

8. See Reference 2, Fig. 30 (c), (f) and (h), p. 116.

9. Ibid, bibliography items 130a, 131, p. 127.

10. J.R. Pierce, Traveling-Wave Tubes, D. Van Nostrand Co., New York, 1950; Figure 5.7, p. 90.

11. J.R. Pierce, "Propagation in Linear Arrays of Parallel Wires," I.R.E. Trans. Electron Devices, vol. ED-2, pp 13 - 24, (1955).

12. See Reference 2, bibliography items 125, 127, 128, p. 127.

13. H.G. Kosmahl and T. O'Malley, "Harmonic Analysis of the Forward-Wave Karp Circuit as a Millimeter-Wave Amplifier in the 100 - 500 W Range," Microwave Power Tube Conference, Monterey, CA, 3 May 1978.

14. A.F.A.L. Contract F 33615-79-C-1737.

15. P.J. Crepeau and I. Itzkan, "An Interaction Circuit for Traveling-Wave Tubes," Proc. IRE (Correspondence), vol. 49, p. 525, Feb. 1961.

16. R.M. White, C.E. Enderby and C.K. Birdsall, "Properties of Ring-Plane Slow-Wave Circuits", IEEE Trans. Electron Devices, vol. ED-11, pp. 247 - 261, June 1964; Figure 1(b), p. 247.

17. Ibid., Figures 2 and 3 (lower left), p. 249.

18. Ibid., Figure 21, p. 258.

19. G. Dube and P. Palluel, "A High-Power Traveling-Wave Tube for C-Band," Proc. 4th International Congress on Microwave Tubes, Scheveningen (Holland), Sept. 1962; pp 79 - 83.

20. H. Desmur, G. Fleury and E.D. Maloney, "160-kW Pulsed S-band TWT," Microwave J. vol. 17, pp. 53 - 56, March 1974.

21. J.E. Field, Ed., The Properties of Diamond, Academic Press, New York, 1979.

22. G.A. Slack and S.B. Austerman, "Thermal Conductivity of BeO Single Crystals," J. App. Phys., vol. 42, pp. 4713 - 4717, Nov. 1971.

23. J. Allison, "A Simple Method for Predicting the Characteristics of Tape Structures," Proc I.E.E., Paper No. 3229E, May 1960 (vol. 107B, pp. 295 - 300).

24. H.J. Curnow, "A General Equivalent Circuit for Coupled-Cavity Slow-Wave Structures," IEEE Trans. Microwave Theory Tech., MTT-13, pp. 671 - 675 Sept. 1965.

25. See Reference 10, Section 5.5, p. 95.

26. W. Hilberg, Electrical Characteristics of Transmission Lines, Artech House Books, Dedham, Mass., 1979.

27. J.F. Gittins, "Power Travelling-Wave Tubes," American Elsevier Publishing Co., New York, 1965; Figure 3.25, p. 67.

28. Reference to Varian production coupled cavity TWTs: VTS-5754, VTR-6625.